Optimizing Real-Time ECG Data Transmission in Constrained Environments

by

Hebatalla Ouda

A thesis submitted to the
School of Computing
in conformity with the requirements for
the degree of Master of Science

Queen's University
Kingston, Ontario, Canada
October 2022

Abstract

ECG monitoring systems have a significant role in detecting cardiovascular diseases and reducing the rate of sudden cardiac deaths through early warnings for heart attacks. One of the critical factors in supporting real-time ECG tracking is to guarantee monitoring system availability. This thesis focuses on battery life extension for a 12 Lead ECG patch utilizing compression and classification approaches.

In the compression approach, the operational hours of the ECG patch are extended by reducing the data size of captured ECG signals to minimize data transmission. Huffman, delta, and base-delta lossless compression techniques are implemented on a Texas Instruments CC2650 Micro-controller Unit using different sampling rates, normal, and abnormal cardiac conditions. The algorithms are evaluated in terms of compression ratio, execution time, and power consumption of the ECG patch.

The computer-aided interpretation of ECG signals has become a pivotal tool for physicians in the clinical assessment of cardiovascular diseases during the last decade. Therefore, computerized diagnosis systems depend heavily on machine learning and deep learning models to guarantee high classification accuracy. With the classification approach, we target effective power consumption by controlling the ECG patch mode of operation to reduce the need for a full-fidelity ECG signal. We use a binary classifier to inform the decision to switch between different operational strategies. In addition, we developed a new approach to support energy-efficient ECG monitoring in real-time through adaptive lead selection for ECG signals to better diagnose different heart conditions.

Our findings show that the base-delta encoding technique outperforms other compression techniques and achieves 70% data compression on normal ECG data, and up to 50% on abnormal ECG data with 24 ms. The adaptive selection of ECG channels with CNN models on 1 and 12 leads achieves 77.7% power saving in the normal cardiac condition and up to 55.5% for the heart blocks, sinus bradycardia, and sinus tachycardia.

Co-Authorship

1. Hebatalla Ouda, Ahmed Badr, Abeulmonem Rashwan, Hossam S. Hassanein, and Khalid Elgazzr. Optimizing Real-time ECG Data Transmission in Constrained Environments. IEEE International Conference on Communications (ICC), 2022 (accepted).

2. Hebatalla Ouda, Abeer Badawi, Hossam S. Hassanein, and Khalid Elgazzr. Energy Saving on Constrained 12-Leads Real-Time ECG Monitoring. IEEE Global Communications Conference (GLOBECOM), 2022 (accepted).

3. Hebatalla Ouda, Hossam S. Hassanein, and Khalid Elgazzr. Adaptive ECG Leads Selection for Low-Power ECG Monitoring Systems Using Multi-class Classification. International Conference on Communications, Signal Processing, and their Applications (ICCSPA), 2022 (under review).

Acknowledgments

First, I would like to thank Allah gratefully for giving me a generous portion of achievements, I would never accomplish the master's journey without his endless blessings.

I would like to express my deepest gratitude to Prof. Khalid Elgazzar and Prof. Hossam Hassanein for their extraordinary support, motivation, mentorship, and guidance. They inspired me to follow the professional attitude of scholars. This two-year journey was a life-changing experience for me with ups and downs. My supervisors gave me the confidence and encouragement at difficult times to continue with a high level of enthusiasm. I am fortunate to work under their supervision and it could not have happened without them.

I was looking forward to this moment to give credit to my lovely parents, my father, Dr. Tarek; my mother, Dr. Wafaa; and my supportive brother, Hossam. They were always providing me with unfailing support, motivation, and continuous encouragement throughout my life and I would never reach anything in life without them.

My grateful thanks are extended to Basia Palmer for her incredible patience and intensive efforts during the master's journey. She is always keen on spreading positive vibes and giving constructive feedback during proofreading. I am thankful for her

continuous support even if we don't request help, she is always there to assure we are motivated to continue.

The journey wasn't easy without spending memorable times with amazing friends. I would like to thank my kindhearted friends: Marah, Sarah, Omneya, Sara Abdelaziz, Shaza, Qamar, Rawan, Eman, Alaa, Mariam, Safa, and Ghada for the truly beautiful moments that we shared during this journey. Furthemore, I am thankful to the ESAQ board: Ahmad Nagib, Alaa, Shaza, Mohammed Anas, as they gave me the opportunity to explore students' activities at Queen's while applying work-life balance.

I would also like to thank all TRL and IoT Lab colleagues, partners of success, for their great support and encouragement towards making a successful and enjoyable academic experience.

Contents

List of Tables

List of Figures

List of Abbreviations

1dAVb 1st Degree AV Block

3D-MRP 3D Magnetic Resonance Pancreatography

ADC Analog to Digital Converter

ANN Artificial Neural Network

APC Atrial Premature Contraction

BLE Bluetooth Low Energy

CALIC Context-based Adaptive Lossless Image Codec

Cloud-MQTT Cloud-MQ Telemetry Transport

CNN Convolutional Neural Network

CR Compression Ratio

DL Deep Learning

DT Decision Tree

DWT Discrete Wavelet Transform

ECG Electrocardiogram

FHIR Fast Healthcare Interoperability Resources

FPGA Field Programmable gate array

HEVC High-Efficiency Video Coding

HL7 Health Level 7

IoMT Internet of Medical Things

IoT Internet of Things

KNN K-Nearest Neighbors

LBBB Left Bundle Branch Block

LR Logistic Regression

LZW Lempel–Ziv–Welch

MAC Media Access Control

Mbps Mega Bit Per Second

MCU Microcontroller Unit

ML Machine Learning

MRI Magnetic Resonance Imaging

PAB Paced Beat

PVC Premature Ventricular Contraction

RAKE Rapid Automatic Keyword Extraction

RBBB Right Bundle Branch Block

ReLU Rectified Linear Unit

RLE Run Length Encoding

RNN Recurrent Neural Network

ROM Read Only Memory

SD Secure Digital

SPS Sample Per Second

VEB Ventricular Escape Beat

VFW Ventricular Flutter Wave

VLSI Very Large-Scale Integration

Chapter 1

Introduction

1.1 Overview and Motivation

During the last 30 years, cardiovascular diseases have been the dominant cause of mortality in more than 195 countries worldwide [1]. The World Health Organization (WHO) reports that “The world’s biggest killer is ischaemic heart disease, responsible for 16% of the world’s total deaths. Since 2000, the largest increase in deaths has been for this disease, rising by more than 2 million to 8.9 million deaths in 2019.” [2]. Developing a real-time electrocardiogram (ECG) monitoring system for cardiac patients is urgently needed to prevent sudden cardiac attacks. ECG data must be collected and transmitted continuously to health care providers in real-time for evaluation.

The Internet of Things (IoT) has contributed significantly to the expansion of healthcare systems during the last decade [3] [4] [5]. IoT technologies play a vital role in supporting ECG acquisition and transmission tasks. Existing efforts in the literature focus on the number of ECG electrodes to acquire data, design of portable ECG patches, transmission mechanisms to deliver captured ECG data between the patch and the cloud, and computational techniques that perform preprocessing on received data before making decisions [6] [7]. The recent ECG monitoring platforms rely on ECG signal classification with high accuracy, especially since the advent of deep learning (DL) techniques. The deep learning models can recognize the various patterns by extracting meaningful features from input data without extensive feature engineering [8]. Moreover, the neural network's performance increases if we use massive training data, which is essential for real-time ECG streaming that generates a large volume of ECG raw data.

The wide range of medical sensors, especially ECG sensors, prompts the need for portable wearable monitoring devices, such as Holter monitor and cardiac events recorders. Holter monitor facilitates continuous cardiac events monitoring for 24 hours, consuming a large amount of power to operate in a constrained environment. Therefore, energy saving is critical in maintaining the sustainability of real-time ECG platforms.

Optimizing energy consumption impacts the durability of ECG monitoring systems. If we reduce the computational power and the overall transmission time to send ECG readings over Bluetooth Low Energy (BLE), we can guarantee seamless continuous monitoring without interruptions due to battery depletion or power outage. To illustrate, if the size of collected ECG data is reduced, the required transmission power will decrease, and the total number of operational hours will increase. Extending the ECG patch operational hours will support continuous monitoring without charging the patch frequently or worrying about ECG readings delivery interruption.

The proposed efforts to date introduce several ways to optimize power consumption during the data acquisition and transmission phases. For example, data size reduction is commonly used in ECG real-time monitoring [9] to reduce the communication overhead required to transfer data between both ends. In addition, changing operational strategies using Machine Learning (ML) and neural network classifiers is another approach to reduce power consumption and support real-time ECG monitoring [10]. Nonetheless, the power consumption evaluation in the low-power ECG monitoring systems that utilize DL models is still underexplored

The remaining research efforts target power consumption optimization by implementing customized hardware circuits [11] or deploying classification on the cloud [12] [13]. As a result, there is a significant gap in testing the performance and durability of the ECG monitoring platforms on real ECG systems. Furthermore, the transmission time of captured ECG data and power-saving analysis on the constrained embedded environments are underinvestigated.

1.2 Problem Statement

The ECG patch processes 13,500 bytes while operating in the high-resolution mode with 500 sampling rate. The high volume of transmitted data increases transmission power which in return consumes the battery of the ECG patch intensively. Efficient techniques to optimize ECG data transmission in a constrained embedded environment remain underexplored. Thus, our thesis targets different power-saving approaches for the clinical assessment of cardiac patients. We aim to address the following research challenges to reduce the power consumption of the target constrained 12-leads ECG real-time platform.

- What are the optimum compression and classification approaches to achieve maximum energy saving with minimum processing and transmission time?

- What is the effect of combining data reduction and switching the mode of operation of the ECG patch on the total power consumption?

1.3 Objectives

This study targets ECG data transmission optimization in a real-time ECG platform and constrained environment. The main objectives are as follows:

- Reducing the amount and size of ECG data needs to be transmitted for diagnostics purposes, while maintaining efficient ECG monitoring.
- Reducing the execution time needed for ECG signals compression to guarantee real-time streaming through the Bluetooth Low Energy (BLE) channel to the internet gateway.
- Evaluating the performance of the commonly used neural models in the literature within the real-time environment.
- Adjusting the number of ECG leads and manipulating the mode of operation of the ECG patch based on the identified cardiac abnormality from CNN models.
- Minimizing the total power consumption of the ECG patch using the adaptive selection of ECG leads.

1.4 Contributions

The main contributions of this thesis can be summarized as follows:

1. We highlight the constraints of real-time ECG platforms that must be considered while optimizing the energy consumption of the ECG patch within embedded environments.
2. We present a quantitative comparison between three mainstream lossless compression techniques including Huffman, delta, and base-delta encoding for ECG signals with respect to compression ratio, execution time, and power saving.
3. We propose to use base-delta encoding as a data size reduction approach to reduce the transmission time and extend the battery life of ECG patches in constrained environments. We also use varying modes of operations to reduce the number of transmitted leads to further save power consumption in normal heart conditions.
4. We evaluate the performance of both data reduction techniques in terms of power-saving and execution time for varying heart conditions on constrained MCU environments.

1.5 Organization of Thesis

This thesis is organized as follows: Chapter 2 provides a comprehensive literature review of the existing contributions to implement ECG monitoring systems, the variety of data compression techniques, the role of ML and DL techniques in ECG classification applications, and the recent efforts to optimize power consumption in cardiac monitoring platforms. Chapter 3 presents the effect of using a data size reduction approach with lossless compression algorithms, such as Huffman, Delta, and Base-Delta encoding on the power consumption of the ECG patch within the TI CC2650 MCU environment. In Chapter 4, we introduce the second approach to reduce the energy consumption using adaptive ECG leads selection. We use binary classification and multi-class classification techniques to support intelligent decision making to change the ECG patch operation mode. Finally, Chapter 5 concludes our work and outlines future directions.

Chapter 2

Background and Literature Review

2.1 ECG Monitoring Systems

The rapid evolution of IoT technologies draws significant interest in real-time ECG monitoring to support patients with chronic heart diseases. In the recent decade, there has been a wide diversity of ambulatory ECG systems that facilitate diagnosis, prognosis, and arrhythmia treatment assessment. Numerous monitoring devices are available on the market with different features, such as backward and looping memory, full disclosure, multi-channels, wearable styles, post-event monitor, and telemetry transmission. Sanders et al. [14] provide an intensive comparison concerning the design, operational duration, cost, advantages, and limitations of recent ambulatory ECG devices like Holter monitor, external loop recorders, implantable loop recorders, mobile cardiac telemetry, patch monitor, and smartwatches as shown in Figure 2.1. Due to the distinct features of each device, the selection of an appropriate ECG monitoring device for the clinical assessment is a critical task to guarantee real-time evaluation, full-disclosure recording, and long recording duration using multiple leads.

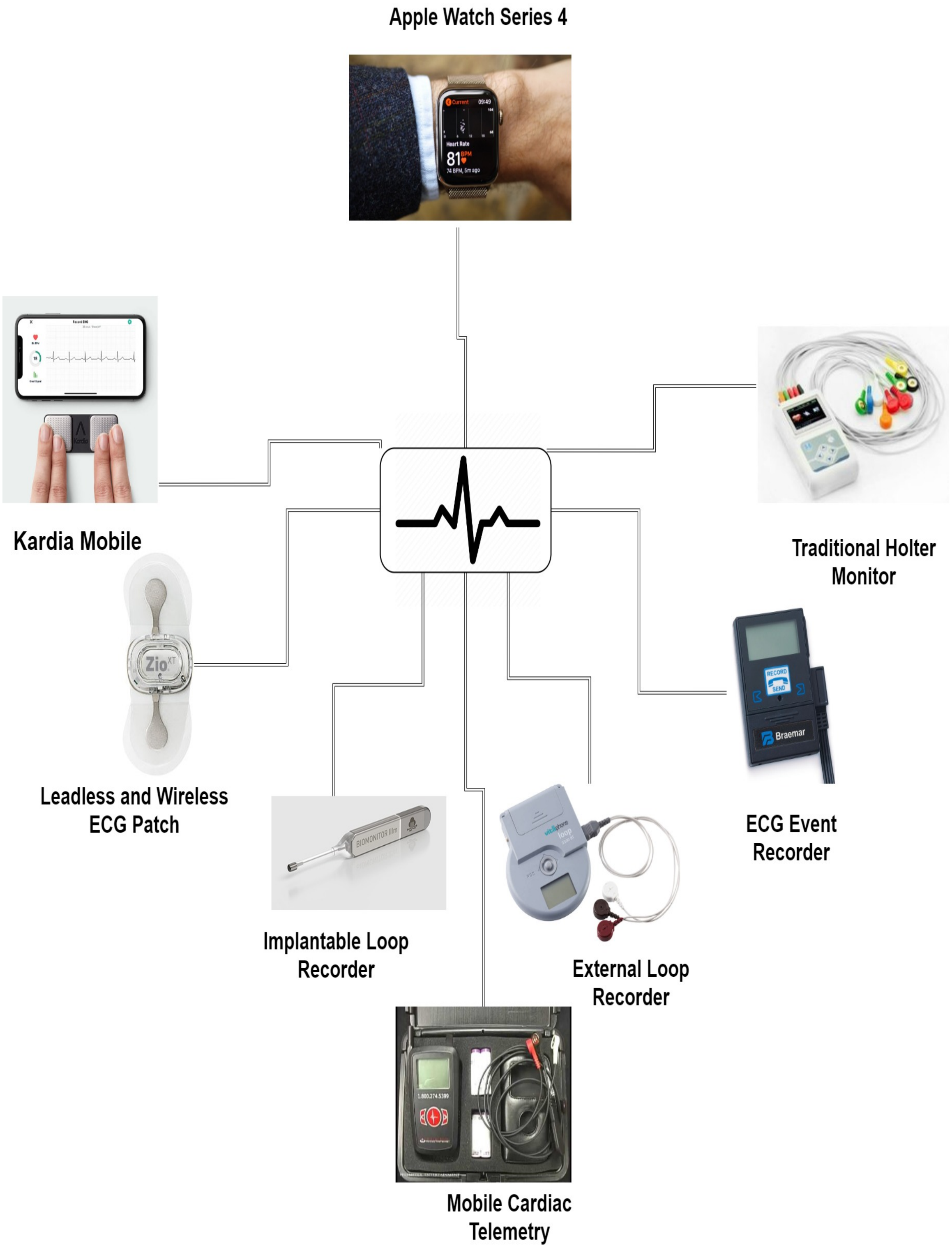

Figure 2.1: Ambulatory ECG devices (Adapted from [14])

Holter monitors, post-event recorders, and smartwatches are the most affordable cardiac monitoring devices. However, post-event recorders and smartwatches require patients activation, which limits their contributions to informational use instead of medical diagnosis, unlike the traditional Holter monitor, which supports continuous ECG monitoring up to 48 hours.

The authors in [6] introduce an overall architecture of ECG monitoring systems illustrated in Figure 2.2 that consists of five layers: acquisition layer, pre-processing layer, modeling and analytics layer, storage layer, and application interfaces layer.

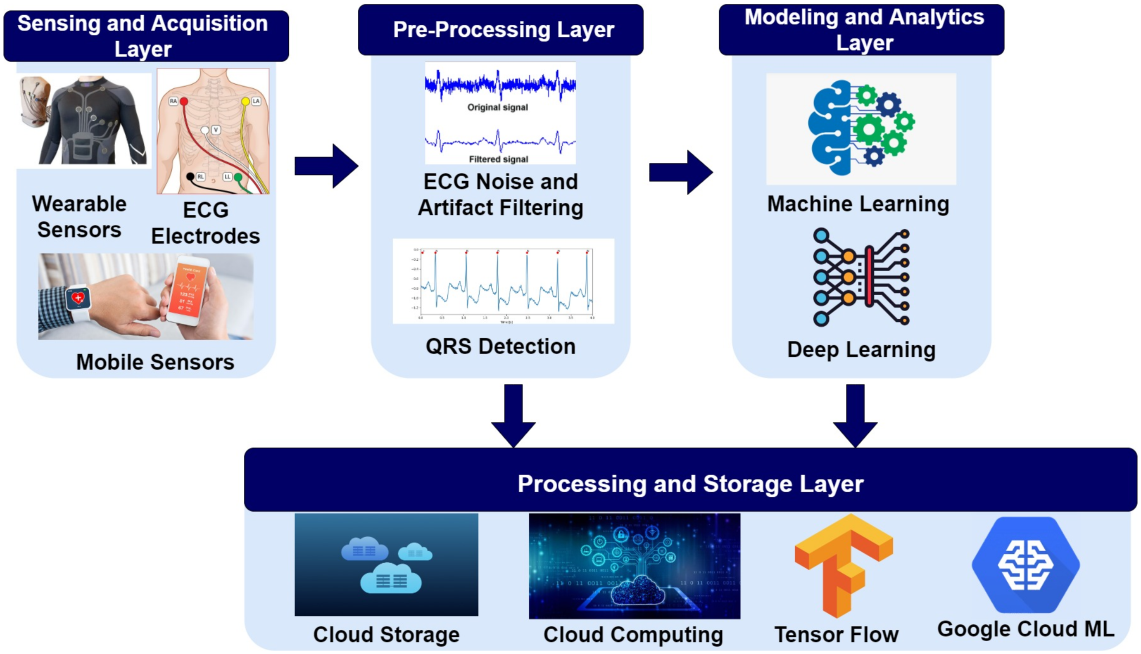

Figure 2.2: The overall architecture of ECG monitoring systems (Adapted from [6])

In addition, Serhani et al. classify the existing ECG monitoring systems in the literature into five main clusters: ECG monitoring context, monitoring technologies, monitoring schemes, monitoring targets, and futuristic monitoring systems as shown in Figure 2.3. Our work integrates CL2, CL3, CL4 and CL5 for an energy-efficient continuous ECG monitoring platform in real-time.

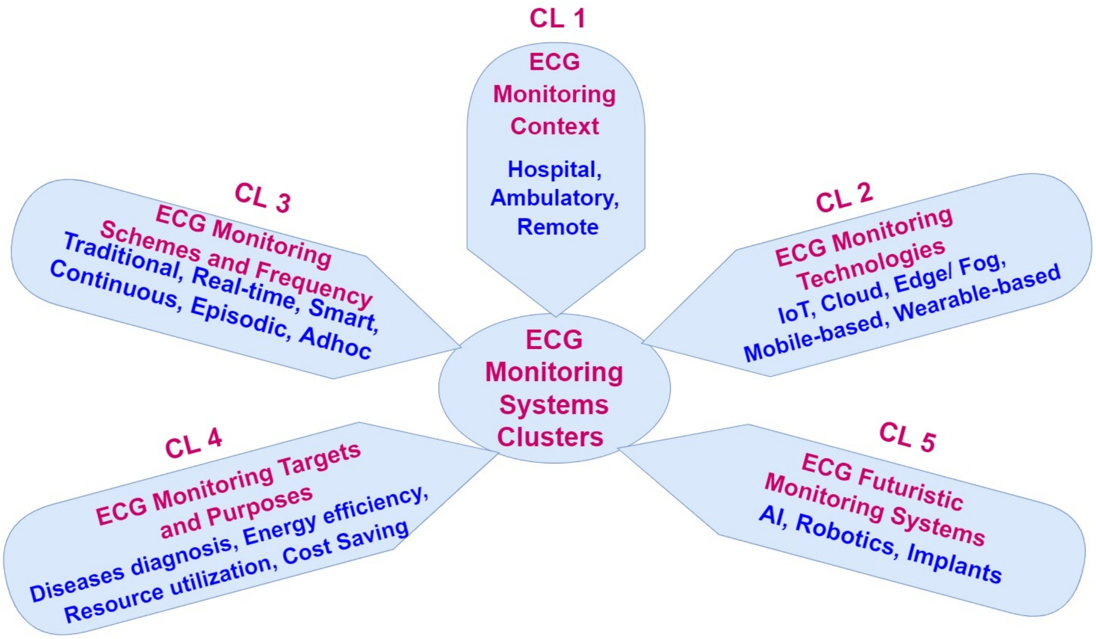
CL 1
ECG Monitoring Context
Hospital, Ambulatory, Remote
CL 3
ECG Monitoring Schemes and Frequency
Traditional, Real-time, Smart, Continuous, Episodic, Adhoc
CL 2
ECG Monitoring Technologies
IoT, Cloud, Edge/ Fog, Mobile-based, Wearable-based
ECG Monitoring Systems Clusters
CL 4
ECG Monitoring Targets and Purposes
Diseases diagnosis, Energy efficiency, Resource utilization, Cost Saving
CL 5
ECG Futuristic Monitoring Systems
AI, Robotics, Implants

Figure 2.3: Clustering of ECG monitoring systems (Adapted from [6])

The existing cardiac monitoring solutions differ regarding the supported features, communication protocols, and the number of ECG patch leads. For instance, some ECG monitoring systems focus on providing primary processes, such as signal acquisition, signal pre-processing, feature extraction, and signal processing [15] [16] [17]. In [18], the heartbeat detection procedure passes through multi-phases starting with signal selection and processing, feature extraction, signal quality assessment, and delay correction. Similarly, the work in [19] focuses on the primary processes like data collection and beat classification while integrating Wireless LAN (WLAN), smartphones, and wearable sensors. The authors produced a smart shirt called Mobile Physiological

Sensor System (MoPSS) that collects physiological data from the wireless body sensor network system (WBSNS), which includes heart rate, body temperature, blood pressure, and blood glucose sensors.

Many efforts have been introduced to support communication between ECG patches and internet gateways. Mishra et al. [20] propose a new method for ECG monitoring based on lightweight MQTT. They collect ECG data using AD8232 Texas Instruments ECG sensor, then transmit collected data using ADS1115 16-bit ADC interface with Raspberry Pi and the I2C protocol. The digital ECG sensor data received from the ADC is published to a Cloud-MQTT broker using a mosquito client based on IEEE 802.11 WLAN. Zigbee has also been used to monitor the ECG status of elderly persons outdoors, giving health care providers the real-time status of their patients [21]. However, the performance of these communication protocols in constrained environments is under-investigated.

Concerning the number of leads, Herry et al. applied a Support Vector Machine (SVM) classification model on the MIT-BIH arrhythmia database to enhance heartbeat detection and classification between normal and abnormal rhythms using a single ECG lead [22]. Similarly, Mathews et al. introduced an approach based on Restricted Boltzmann Machine (RBM) and deep belief network (DBN) methodologies to classify ventricular and supra-ventricular heartbeats using a single ECG lead [23]. Their proposed work is limited to single-lead only with offline processing, while our platform aims to capture 12-lead ECG data to cover a wide range of cardiac issues in real-time.

Walinjkar and Woods integrated a wearable three-lead ECG monitoring kit with a real-time arrhythmia classification and prediction model to send notification alarms while uploading the collected data to the database using HL7 and FHIR standards

[24]. Although the authors claim that their approach supports real-time monitoring, they have a limited number of leads to capture precise ECG signals in abnormal conditions. A flexible 12-lead Holter monitor is proposed [25] using an STM32F microcontroller to support long-term monitoring. This Holter monitor facilitates digital compression at stages close to the acquisition phase to overcome limitations of coverage and bandwidth of cellular networks. However, their approach does not provide real-time updates and notifications to healthcare providers when abnormal conditions are detected.

Other monitoring systems [26] [27] provide advanced processing and add more supporting features such as visualization, compression, data storage, and encryption. As an example, Alex et al. [28] propose a fully homomorphic encryption (FHE) algorithm to encrypt the collected ECG data and assure safe storage of patients' data on the cloud before being processed and sent to the doctors for medical assessment.

2.2 Data Compression Techniques

The advancement of IoT applications led to an exponential growth in the volume of generated data. As a result, more storage capacity and computational power are needed to transmit the massive volume of ECG data to the internet gateway, which is detrimental for real-time applications. Therefore, data size reduction using compression is used to minimize the total consumed energy and the required memory in healthcare applications.

Data compression techniques are classified into two types: lossy and lossless algorithms. In lossy algorithms, part of the data is lost after decompression. Conversely, lossless algorithms reconstruct the original data without any loss. Lossy algorithms, such as Transform Coding, Discrete Cosine Transform, Discrete Wavelet Transform, and Fractal Compression, are used with multimedia data (e.g., images, audio, and video) and limited non-life-threatening healthcare applications [29], while lossless algorithms, such as Run Length Encoding, Lempel–Ziv–Welch (LZW), Arithmetic Encoding, Huffman Encoding, and Shannon Fano Encoding are used with textual data [30]. In wireless sensor networks, there are five categories of compression techniques [31]: string-based, image-based, compressed sensing, distributed source coding, and data aggregation. String-based, image-based, and compressed sensing are commonly used techniques in the healthcare domain [32] [33] [34].

Lossless compression techniques are vital in sensitive healthcare applications like arrhythmias detection and heart attack prediction [35]. The lossless approaches eliminate the risk of losing any part of the ECG recordings that could contain critical information for medical evaluation.

We will demonstrate the existing lossless algorithms in the literature and focus on the lightweight techniques that we used in our constrained embedded environment.

2.2.1 Run-Length Encoding (RLE)

RLE is a lossless compression technique widely used in image- based, and animation applications [36] [37]. RLE represents the number of occurrences for each symbol in the data sequence. Accordingly, RLE is efficient for data with high local correlation. However, the decompression process takes a long time and produces low decompression bandwidths. Kanania and Padole [38] utilize the RLE algorithm to apply parallel encoding on large Genome files within a distributed Raspberry Pi environment. They detect abnormal patterns in genetic files while reducing the computational power due to the compression output. The biosignal compression toolbox is introduced in [39] to support data recoverability. The authors merge transformation methods and encoding techniques, such as Huffman encoding and RLE, to create a compression pipeline on wearable ECG sensors, photoplethysmography (PPG), accelerometry, and skin temperature. The compression pipeline is evaluated in terms of compression ratio and Percent Root-mean-square Difference to recommend the efficient transformation and encoding methods for each wearable sensor.

2.2.2 Lempel–Ziv–Welch Encoding (LZW)

LZW encoding is one of the dynamic dictionary-based techniques. Each dictionary element starts with the last letter from the previous dictionary item. The encoding output is the index of dictionary records. The drawback of the LZW encoding technique is the long processing time to construct the entire dictionary. Wilson et al. [40] implement a novel feature extraction technique using LZW Probabilistic Finite State Automata (LZW-Coded PFSA) to recognize the distinct human activities accurately with 95.6 % classification accuracy. A benchmark suite for the Internet of Medical Things (IoMT) called HERMIT is introduced to ease the evaluation of microarchitectures in IoMT applications [41]. LZW encoding is deployed in HERMIT to represent the compression component in IoT devices while transmitting medical sensor readings over the network.

2.2.3 Arithmetic Encoding

Arithmetic encoding is an entropy-based technique that encodes data strings in two phases [42]. First, the string is mapped into a floating point range, and this step is repeated recursively for all string characters. Second, the floating point range is translated into binary sequence. The Arithmetic approach is used for image compression and secure biometric applications. In [43], the authors introduce a novel image compression technique using block-based arithmetic encoding to select the threshold for prediction and choose the optimal block size of the residual image. Their approach outperforms other lossless image compression techniques, such as CALIC, JPEG-LS, HEVC and 3D-MRP. Aparna et al. [44] propose fingerprint biometric authentication. They use arithmetic encoding to generate a watermark image for the MRI images by encoding the image data and combining the encoded stream with the original input.

2.2.4 Huffman Encoding

Huffman encoding is a leading lossless algorithm and widely used in most text-based applications [45][46]. In Huffman encoding, every character in the original message is represented by binary code after generating the Huffman tree [47]. The length of binary codes depends on the frequency (i.e., times of occurrences) of each character. Huffman encoding was our first choice to apply compression on collected ECG data because of its superior compressing capabilities to the lossless compression techniques. It efficiently reduces the original data size by assigning short codes for most repeated characters and longer codes for less repeated characters. The majority of the previous works implement the Huffman algorithm on PC as a software compression solution, while a few contributions run the Huffman algorithm on embedded systems using

FPGA and VLSI[48][49].

2.2.5 Delta Encoding

Delta encoding is one of the simplest compression techniques for storing and transmitting data. Ideally, delta compression works best when the consecutive samples are very similar. It outperforms Huffman compression for data redundancy elimination when small changes occur between sequential samples [47]. There is limited usage of delta encoding with ECG in the literature. Existing contributions integrate delta encoding with adaptive Huffman to compress static MIT-BIH database [50]. We apply delta encoding as a standalone technique on a stream of collected ECG data in real-time.

2.2.6 Base-Delta Encoding

. Base-delta encoding is a modified version of the delta algorithm that measures the difference between the first sample and the remaining samples to reduce the original message size. It was introduced in 2012 to reduce caching size [51]. In this work, we utilize base-delta to compress ECG data and obtain compressed samples with varying lengths compared to the fixed byte size in delta compression.

In this work, we aim to compress ECG data after the acquisition phase to reduce the size and the transmission power required to send this data. Accordingly, we are interested in applying lossless algorithms to time series ECG data, such as Huffman encoding, delta encoding, and base-delta encoding. Our approach targets real-time data compression with stringent execution time to satisfy resource-constrained system specifications (computation and energy) and meet real-time application requirements. It is important to enable real-time notifications when abnormal conditions are detected.

2.3 ECG Signals Classification Techniques

2.3.1 Binary Classification

Due to the high demand for accurate detection and early prediction of ECG cardiac risks, the recent ECG monitoring platforms include machine learning approaches for identifying and classifying cardiovascular diseases. Supervised and unsupervised learning techniques are used in ECG platforms for different purposes [52]. For instance, diagnosis applications mainly depend on supervised learning approaches, while unsupervised learning approaches are used for automatic risk detection applications that need unknown physiological feature discovery.

Wasimuddin et al. [53] propose an intensive review of the existing research efforts in implementing multi-stages ECG signal analysis models using traditional and advanced ML techniques. The stages-based model consists of four phases: dataset sources, quality check, feature engineering, and classification. Likewise, Luz et al. [54] review the published contributions in ECG acquisition methods, datasets, preprocessing methodologies, segmentation, feature extraction techniques, and learning algorithms.

In [55], the researchers apply the threshold-based methodology to the European ST-T database to detect cardiac ischemia. Although their approach achieves 98.12% average sensitivity and 98.16% average specificity, the processing pipeline consumes too much time, which is critical for real-time systems. A polynomial regression model is proposed in [56] to detect acute myocardial infarction. The regression model is deployed on ECG data collected from 12 leads for 10 seconds. The classifier reaches 97% sensitivity, but the dataset is small to obtain a full performance evaluation similar to the real monitoring systems. Signal analysis and feature generation are essential before handling classification tasks. Thus, Li and Zhou [57] apply wavelet packet decomposition on the MIT-BIH arrhythmia database to decompose the approximations and details of the ECG signal and represent the critical information in higher-frequency components. The representative features are extracted after entropy calculations on decomposed components. The Random Forest model utilizes the generated features and achieves 94% classification accuracy. The authors compare their approach and the published approaches in terms of accuracy and execution time. Their technique outperforms Support Vector Machine (SVM), K-nearest neighbours (KNN), Decision Tree (DT) and Probabilistic neural network algorithms which make their model a promising solution for continuous monitoring platforms. The work in [58] categorizes the automated methods to detect myocardial ischemia and infarction based on the number of used leads, such as V1, V2, V3, V4, V5, I, and II, the feature selection methods like Forward feature selection (FFS), Evolutionary optimization algorithms, Feature weighting approaches, and Fuzzy rough feature selection. Furthermore, Ansari et al. review the classification methods starting from simple thresholding and traditional ML algorithms like SVM, KNN, and DT to convolutional neural networks (CNN), rule-based expert systems, and neuro-fuzzy classifiers.

ECG signals classification with SVM is widely used in the literature. For instance, Venkatesan et al. [59] apply SVM on the MIT-BIH arrhythmia database to detect normal and abnormal cardiac conditions based on the heart rate variability (HRV) feature. Despite the high classification accuracy of the SVM model, which reaches 96%, the experimental work is introduced using a MATLAB simulator with a high processing time above 20 seconds which restricts the model usage to cardiac events recording only without real-time monitoring features. Equivalently, the cardiac arrhythmia detection using SVM is proposed in [60] with 99.2% classification accuracy. The authors implement the classification pipeline starting with pre-processing, R-R peak detection, Q- wavelet transform for feature extraction before training the SVM classifier on the MIT-BIH arrhythmia database.

2.3.2 Multi-Class Classification

The ECG monitoring systems have significantly improved after emerging deep learning techniques. Deep neural networks play a vital role in providing accurate and fast diagnoses for a wide range of cardiac diseases. Accurate ECG classification is clinically essential to predict and control cardiac patients before suffering from critical side effects and deterioration. Unlike the traditional machine learning algorithms, deep learning algorithms could handle data pre-processing, feature extraction, and classification efficiently on large data volumes.

In the literature, many efforts are introduced to support ECG diagnosis using deep learning [61] [62] [63] [64]. The existing solutions for abnormal ECG detection differ in terms of the diagnosis type, DL algorithm, and the used datasets. There are different types of diagnosis applications that rely on DL models. For example, myocardial infarction detection, arrhythmias detection, irregular heart rhythm classification, and coronary artery classification are different ECG diagnosis types. The convolutional neural network (CNN) and recurrent neural networks (RNN) are the commonly used DL algorithms in diagnosis applications. The used datasets vary between the MIT-BIH arrhythmia database, PTB-XL dataset, PhysioNet Cardiology Challenge 2017 dataset, European ST-T dataset, INCART dataset, and Self-constructed datasets.

Some of the existing solutions focus on the hardware used in training the neural networks. For instance, Wu et al. [65] introduce a lightweight neural network-based ECG classification algorithm with high recognition accuracy by combining both the bi-directional long short-term memory (BLSTM) and convolutional neural networks (CNN). The authors utilize a high degree of similarity between successive heartbeats to achieve computation reuse on hardware architecture which speeds up the network inference and improves the energy efficiency. However, the proposed processor is not for continuous ECG monitoring. Although they reuse the repeated cardiac cycles to minimize the computational power and save energy, this technique could lead to additional delay, which contradicts real-time ECG streaming. Correspondingly, Janveja et al. [66] propose an initial prototype for wearable ECG monitoring. They fabricate an additional processor unit to handle multi-class classification using DNN and MIT-BIH datasets. The Co-Processor consists of 2 main blocks: Pre-processing with a beat extraction block and a classification block. They minimize the computational complexity by reducing the total number of input and hidden layers, which leads to minimizing power consumption. Despite the main goal of using the energy-efficient processor, the energy-saving analysis for the different classified classes using the customized co-processor is missing. Corradi et al. [67] introduce a method for encoding and compressing ECG signals into a stream of asynchronous digital events.

The compressed ECG signals can be correctly classified into one of 18 classes after a dimensionality expansion performed by RNN. The authors use a software simulation compatible with a digital embedded implementation. After the simulation results, they fabricate a custom mixed-signal analog/digital neuromorphic processor to implement the recurrent SNN. The authors aim to reduce the power consumption while training the RNN using the VLSI neuromorphic processor, but there is no explanation of how they evaluated or reduced the power consumption. According to work proposed by Monedero [68], a functional ECG diagnosis system could perform an accurate medical assessment by following a specialist's approach. The author uses a set of rules in the system to differentiate 13 diseases with a high-reliability rate. Five leads (I, II, V1, V5, and V6) are used instead of a standard 12-lead ECG to perform the diagnosis. A novel noise indicator is deployed to measure the quality of the acquired ECG signals, which allows repeating the ECG recording if the noise level is high and cannot be filtered. Furthermore, signal processing techniques are applied to captured signals for wave identification and Chi-squares Automatic Interaction Detection (CHAID) model detects 13 cardiac risks. The proposed system depends on signal processing techniques; it will need large memory to store records besides the high computational delays, which act as a barrier to supporting real-time ECG monitoring. Hybrid architectures, such as Long Short Term Memory (LSTM) cells and Multi-Layer Perceptrons (MLP) are merged in [69] for ECG anomaly detection on the MIT-BIH arrhythmia database. Sivapalan et al. recommend data augmentation using Synthetic Minority Oversampling TEchnique (SMOTE) to solve the unbalanced classes in the dataset. Energy saving is achieved according to the following scenario:

Once an ECG beat is identified as anomalous, the wireless transmission will be enabled, thus reducing sensor power consumption. Nevertheless, the ANN technique increases the current consumption. In addition, continuous real-time ECG transmission is not supported as ECG readings are only transmitted if an anomalous beat is detected.

2.4 Power Optimization in ECG Platforms

The recent decade has witnessed an increased demand for portable real-time ECG monitoring systems [6] [70]. Efficient ECG monitoring platforms are concerned with data acquisition techniques, compression transmission approaches, models for accurate diagnosis, and energy-saving methods while defining the design specifications for real-time systems. In addition, there are required components that have to be considered while designing wireless ECG monitoring systems [71], as shown in Figure 2.4, where power consumption is one of the vital components to guarantee the system's availability.

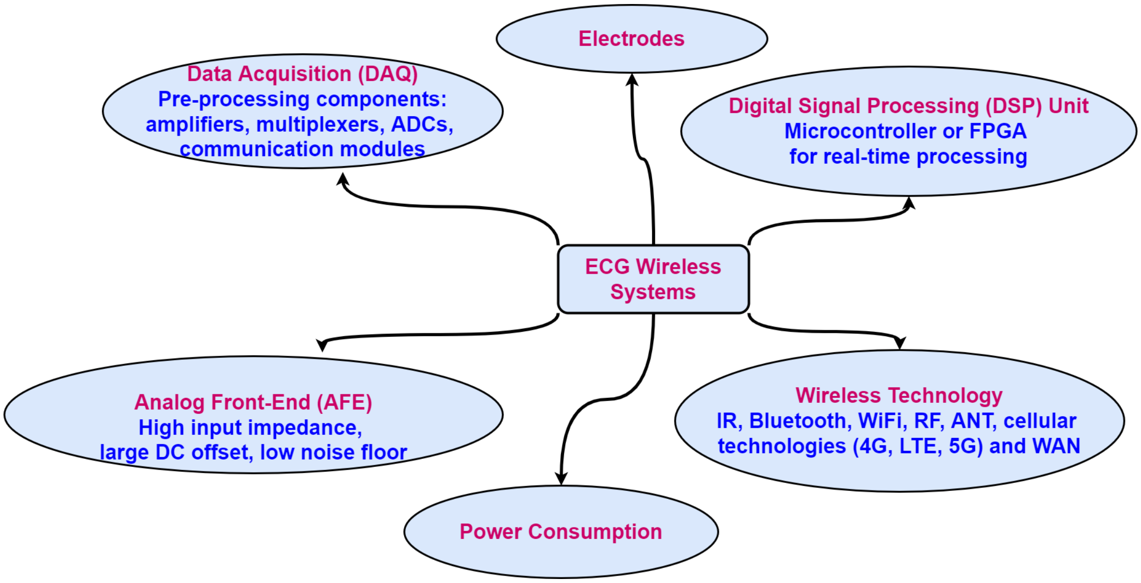

Figure 2.4: Design components of ECG wireless systems

Optimizing energy consumption in health monitoring systems attracts significant contributions to support continuous physiological measurements. Accordingly, existing research efforts differentiate between the energy demand and supply concepts to manipulate energy saving on continuous monitoring platforms [72].

1. *Energy Demand*: The rapid evolution in continuous monitoring platforms generates great interest in evaluating the total energy consumed by wearable sensors [73] [74] [5], signal pre-processing circuit modules [75], memory modules [76], and wireless communication modules [77] [78].

2. *Energy Supply*: To accommodate the increase in energy demands, self-powered techniques are introduced to maintain a stable power supply during the data acquisition, processing, and transmission phases. For instance, energy storage using flexible batteries and supercapacitors facilitates portable power sources for wearable systems [79] [80]. Furthermore, energy harvesting opens the door

for renewable energy usage [81] and obtaining the necessary power from human thermal energy and body movements [82].

There are limited contributions in the literature that address the impact of real-time data acquisition, signal processing, and data transmission on the power consumption of ECG monitoring devices. The majority of these contributions aim to minimize the required computational power by reducing the data size and wireless transmission time.

Data size reduction is achieved by applying lossy or lossless compression algorithms on ECG signals [83]. Moon et al. investigate a way to balance data reduction and data fidelity on ECG data received from the BioSemi Active Two system devices using discrete cosine transform (DCT), discrete wavelet transform (DWT), and R-peak validation [84]. Similarly, Rebollo-Neira in [85] evaluates DWT as a simple lossy compression technique on the MIT-BIH arrhythmia database. However, DWT achieves a high compression ratio with negligible delay. In both contributions, the experimental work is not tested on a real ECG system or a constrained platform to evaluate the performance and energy-saving at low distortion recovery. Reducing transmission time through lossless compression is proposed by Tsai et al. in [86]. The authors propose three separate techniques: (1) an adaptive linear predictor that selects the best ECG readings to decrease the prediction error, (2) an improved context-adaptive Golomb-Rice code for data storage optimization, and (3) a fixed-length packing format to decode data in real-time. The authors compare the linear predictor and the remaining lossless algorithms in terms of compression ratio, but the transmission time and power-saving analysis are missing on the embedded platform. Campobello et al. [85] introduce a simple lossless algorithm named RAKE to encode the binary representation of an ECG signal during the pre-processing phase. The RAKE algorithm achieves a compression ratio of 2.67% compared to 2.43% in Huffman and 2.25% in Dynamic Pack. However, RAKE produces a high latency equal to 500 ms as it operates on data blocks that are too high to meet the real-time demands in constrained environments. In a few works, lossy and lossless techniques are combined to create a hybrid approach. Deepu et al. demonstrate this hybrid encoding system to control the transmission mode, and power consumption in IoT-enabled wireless sensors [87]. Despite the resulting high energy saving ratios, the implementation complexity depends on the selected lossy and lossless schemes. Furthermore, the compressed data needs to be decompressed locally at the sensor node, which demands more storage and causes additional delay.

ECG classification algorithms support making the appropriate decision to switch to lower data fidelity mode which reflects on energy-saving for real-time platforms. For instance, Kung et al. [88] recommend the Random Forest (RF) algorithm with 98.63% classification accuracy for energy saving in ECG systems. They compare RF and other QRS detection algorithms in terms of sampling rate and sensitivity. Nonetheless, their work lacks a practical performance evaluation on real-time monitoring systems. Multistage pruning CNN achieves 97% accuracy in low-power ECG classification and a 60.4% decrease in run-time complexity [89]. On the other hand, CNN requires high computational power that renders its deployment on low-powered edge nodes unrealistic for real-time applications. Wang et al. [90] introduce an energy-efficient scheme for wearable ECG monitoring that consists of two processes: adaptive compression and neural network. In adaptive compression, the authors combine lossy and lossless techniques and switch between both based on the classification results from a tree-structured neural network (TSNN). The scheme scored 98.4% in diagnosis accuracy and a 99.9% reduction in computational complexity, which in turn reduced the power consumption. One drawback of this scheme is the overall latency due to the execution time of the two processes. Such a delay prevents effective real-time ECG diagnosis. In [91], dynamic management of the Internet of Medical Things (IoMT) nodes is defined using a hardware/software development template. Scrugli et al. control the operation modes of IoMT nodes based on the results of quantized CNN using the MIT-BIH database. They could save energy by manipulating the hardware and software components of the ECG device, such as capturing raw data, peak detection, and CNN processing.

The effect of using a renewable energy approach on the power consumption of ECG devices is investigated in [92]. Bui et al. designed a solar-powered ECG device to achieve optimal power consumption and maintain system availability without needing battery replacement. The fabricated ECG device contains solar harvesting modules to store energy at night with super-capacitors. Additionally, it operates with a range of sampling frequencies up to 2133 Hz to facilitate communication with a wide range of smartphones and low-powered devices. The solar-based design reduces power consumption significantly with a 1.9 V supply. However, the solar-powered ECG device can capture ECG signals from five leads maximum which is inefficient for critical monitoring applications like arrhythmia detection which requires readings from all 12 leads.

Chapter 3

Data Size Reduction With Lossless Compression

3.1 Motivation

The rapid growth of e-healthcare solutions leads to a significant increase in connected medical devices, which is expected to reach 75 billion by 2025 [93]. Health monitoring devices generate a large amount of data continuously, which is considered a challenge for system availability. For instance, the ECG Holter monitor produces 135000 bytes each second while recording the changes of ECG signals at a 500 sampling rate. The transmission of huge data volumes causes high power consumption and rapid battery discharging, which negatively affects the continuous cardiac events recording. To reduce the total power consumption, we need to minimize the transmitted data size using the compression approach. In the literature, there is a wide range of lossy and lossless techniques for ECG applications. Due to the sensitivity of ECG data and to eliminate the risk of losing important part of the captured signals, we use lossless compression techniques. In this chapter, we aim to optimize the power consumption of ECG patches in the constrained embedded environment by applying different lightweight lossless compression techniques.

3.2 System Overview

Our proposed platform [94] is functionally divided into five phases: data acquisition, data transmission, data storage and streaming, data processing, and data analytics and decision-making phase, as shown in Figure 3.1. In the data acquisition phase, we capture the analog ECG signals from 10 electrodes before being converted to the digital format using the ADS 1298 chip. The digital ECG signal is compressed on the TI CC2650 MCU prior to being sent over the BLE to the internet gateway in the transmission phase. The electrocardiogram readings will be streamed using data streaming engines and stored to keep the recordings available for further processing. In the final phase, ECG signals are classified using deep learning models, and then healthcare providers will be notified based on the analysis.

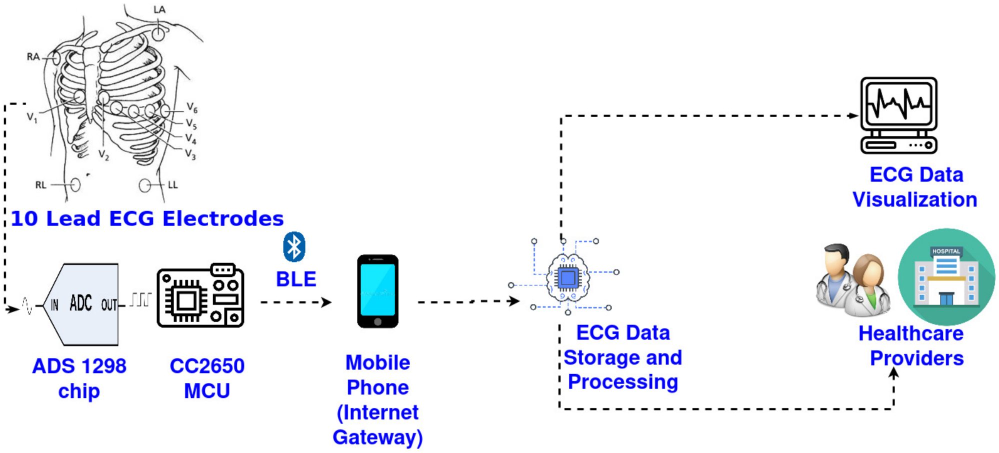

Figure 3.1: System architecture of the real-time ECG monitoring platform

3.3 System Requirements

The data acquisition task runs at a sampling rate from 250 to 500 SPS. During the 250 SPS, the acquisition task captures a single sample every four milliseconds, that is, 250 samples/1000 ms = 4 ms. To capture each sample, the data acquisition task needs 1 ms. Leaving the remaining time for other tasks including compression, data logging, and transmission to progress after every sample acquisition, which amounts to 3 ms (4 ms - 1 ms). At 500 SPS the time is 1 ms. However, in our system samples are processed in groups every 1 s, during this period the logging and transmission tasks must be completed. When the sampling rate is 250, we have 750 ms available for these two tasks. By comparison, at 500 SPS, there are 500 ms available to complete the tasks. In our system this operation is under a stringent time constraint, leaving data logging and transmission tasks having to be completed within 750 ms. If not completed, these tasks will be interrupted by the data acquisition task as data acquisition has the highest priority in our system to ensure data is not missed. The ECG hardware firmware condenses the MCU operations into three separate tasks: data acquisition, data logging, and data transmission using the scheduling APIs of the onboard RTOS. Each task is classified based on a predetermined hierarchy. In the firmware operating on the hardware the data acquisition task receives the highest priority followed by the data logging task which has the second-highest priority, and lastly, the data transmission task has the lowest priority.

To that extent, the following objectives are set to deliver the expected outcomes by the ECG acquisition hardware:

1. Reduce the digitized ECG data size before transmission over BLE to the backend system.

2. Maximize the ECG acquisition hardware battery life by enhancing the power consumption profile of the device.

3.4 Experimental Setup

The experimental environment setup consists of the following steps:

1. Collect ECG signals in real-time from the heart simulator. The CC265x powers the hardware to acquire the ECG signals in real-time from the heart simulator under six different heart conditions: normal heartbeats at 92 bpm, abnormal ventricular tachycardia, atrial premature contraction, right bundle block, premature ventricular contraction, and ventricular fibrillation heartbeats.

2. Create two test environments by constructing two buffers, where the buffer sizes are 1000 and 500 samples. The buffers carry equivalent ECG data of two seconds at 500 SPS and 250 SPS, respectively.

3. Apply Huffman, delta, and base-delta encoding compression techniques on the buffered data in two operation modes. The first operation mode is when the data acquisition hardware is working offline, which means the radio module for BLE is turned off, and the data transmission task is not scheduled. This simulates when the ECG patch is disconnected for any reason. The second mode is the real-time continuous operation mode, where the collected ECG data is compressed, saved on a local SD storage, and transmitted to the nearest paired BLE device.

4. Compare various compression techniques in terms of compression ratio and execution time.

5. Calculate the energy-saving after applying the compression techniques to the constrained system.

3.4.1 ECG Datasets Acquisition

To collect ECG data, we connect our data acquisition platform to the TechPatient CARDIO V4 ECG simulator [95] as shown in Figure 3.2. The simulator can generate real-time ECG waveforms for different cardiac conditions. It supports two modes of operation, ECG mode and rhythmic mode. The ECG mode provides a realistic 12-leads ECG waveform. The rhythmic mode simulates 45 predefined heart diseases including arrhythmias, such as ventricular tachycardia and ventricular fibrillation. Using the ECG simulator, we created six different datasets: normal ECG, ventricular tachycardia, ventricular fibrillation, atrial premature contraction, premature ventricular contraction, and right bundle block. Each dataset contains a total of 30 minutes of ECG waveform recordings.

Figure 3.2: TechPatient CARDIO V4 ECG simulator

3.4.2 Dataset Characteristics

Our ECG data is acquired at sampling rates between 250 - 500. Each sample contains the data of eight ECG channels. Every ECG channel carries 24 bits of raw data, plus an additional 24 bits representing the status of the electrodes attached to the patient's body (i.e., whether they are correctly connected or not). Respectively, one successful sample holds 216 bits of information (8 channels * 24 bits for data + 24 bits for electrode status). As a result, our ECG patch processes 6750 bytes per second while operating in the low-power mode at a rate of 250 SPS and 13,500 bytes while operating in the high-resolution mode at a rate of 500 SPS.

3.4.3 ECG Data Reduction

To transmit data over a wireless interface, the power consumption rate is proportional to the volume of transmitted data. As indicated above, our ECG patch generates a large volume of data each second, which requires a large amount of power to transmit. Theoretically, if we reduce the data size, we consume less power to transmit, given that we have the computational capacity to do so within the constrained time budget. Thus, we use lightweight lossless compression algorithms to increase battery life and extend the ECG patch operational hours for efficient real-time monitoring. We implement the Huffman, delta, and base-delta encoding algorithms using embedded C in TI Code Composer Studio for the TI CC265 MCU and compare the performance of each algorithm to determine the appropriate technique suitable for the system requirements.

3.4.3.1 Huffman Encoding

In this scenario, we implemented the Huffman algorithm to accept the raw ECG signal as input before building the Huffman tree. To generate the Huffman tree, the frequency of each character is calculated and sorted in ascending order. The minimum two frequencies are merged to be one tree node. Fetching the least frequencies is repeated recursively to build the entire tree as shown in the pseudo-code below:

Algorithm 1 Huffman Encoding

```
n = C.size
Q = priority_queue()
for $i = 1 \dots, n$ do
    n = node(C[i])
    Q.push(n)
end for
while $Q.size() \neq 1$ do
    Z = new node()
    Z.left = x = Q.pop
    Z.right = y = Q.pop
    Z.frequency = x.frequency + y.frequency
    Q.push(Z)
end while
Return Q
```

For each non-leaf node, we assign 0 to the left edge and 1 to the right edge. We insert the characters and the equivalent binary representation in a hash table where the most frequent characters are represented with fewer digits. We will discuss the way of calculating the Huffman encoding compression ratio in the results section.

3.4.3.2 Delta Encoding

In the delta encoding algorithm, we calculate the difference between each consecutive sample rather than sending the exact large-size samples which reduces the original data size. The resulting output contains the first original samples followed by deltas for the remaining successive samples as described in the pseudo-code below:

Algorithm 2 Delta Encoding

```
base = 0
current_sample = first_sample
for $i = 0 \ldots, n\_samples$ do

    if $result\_counter$ == 0 then
        result = current_sample - base
        Result[result_counter++] = result
    else
        result = next_sample - current_sample
        Result[result_counter++] = result
    end if
end for
```

3.4.3.3 Base-Delta Encoding

In this scenario, we select the first ECG sample to act as a baseline. We subtract the rest of the samples from the base value to get a new data buffer. Accordingly, we send a buffer of deltas with the base value instead of the original values as shown in the pseudo-code.

Algorithm 3 Base-Delta Encoding

```
base_value = ECG_samples [0]
for $i = 0 \ldots, n\_samples$ do
    current_sample = buffer[i];
    Result[i] = base_value - current_sample;
end for
```

3.4.4 Hardware Specifications:

All compression algorithms we targeted during this study were implemented using embedded C on the Texas Instruments CC2650 microcontroller chip in Figure 3.3.

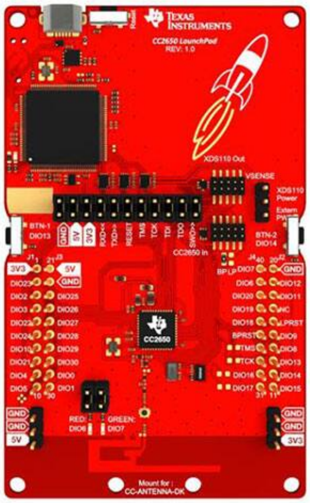

Figure 3.3: CC2650 SimpleLink multistandard wireless MCU

TI CC2650 is a SimpleLink Multi-standard Wireless MCU supporting Bluetooth, ZigBee and 6LoWPAN, and ZigBee RF4CE protocols which make it an ideal choice for medical, industrial, remote control and wireless sensor networks applications. CC2650 board is a member of the CC26xx family of cost-effective, ultra-low power, 2.4-GHz RF devices. The CC2650 device contains a 32-bit ARM Cortex-M3 processor that runs at 48 MHz as the main processor and a rich peripheral feature set that includes a unique ultra-low power sensor controller. TI CC2650 is equipped with a Bluetooth Low Energy controller and the IEEE 802.15.4 MAC that are embedded into ROM and are partly running on a separate ARM Cortex-M0 processor. This architecture improves overall system performance and power consumption and frees up flash memory for the application.

3.5 Lossless Compression Results

3.5.1 Data size Reduction - Execution time Trade-off

To evaluate the performance of each encoding technique within the constrained embedded environment of TI CC2650 MCU, we need to compare the amount of data reduction with the required processing time for each algorithm. The compression ratio (CR) represents the reduction in data size produced by the compression algorithm. To obtain the compression ratio we divide the data size after compression by the data size before compression as follows:

$$\mathbf{CR} = 1 - \frac{\text{data size after compression}}{\text{data size before compression}} \tag{3.1}$$

Based on the system requirements, the execution time of each compression algorithm is a critical factor as we need 40 ms maximum to execute compression tasks on the MCU in real-time. As the TI CC2650 has crystal frequency = 32 kHz (i.e., 32000 ticks /second), the total time to run the compression task is calculated as follows:

$$\textbf{Execution Time (ms)} = 1000 \times \frac{\text{Timestamp interval before and after the execution}}{32000} \tag{3.2}$$

We run Huffman, delta and base-delta encoding using two different sampling rates to accommodate various operation modes on the ECG patch. In Tables 3.1 and 3.2, we compare the compression algorithms' performance in terms of the compression ratio where the buffer size equals 1000 and 500 samples (i.e., collecting ECG data for 2 seconds using 500 and 250 sampling rates).

Table 3.1: Compression ratios of lossless encoding algorithms with buffer size = 1000 Samples

ECG Signal	Huffman Encoding	Delta Encoding	Base-Delta Encoding
Normal	84.9%	72.3%	73.6%
Ventricular Tachycardia	56.1%	0%	44%
Ventricular Fibrillation	56.7%	0%	41.7%
Atrial Premature Contraction	53.1%	1.5%	51.8%
Premature Ventricular Contraction	52.3%	1.2%	50.6%
Right Bundle Block	51.7%	0%	55.4%

Table 3.2: Compression ratios of lossless encoding algorithms with buffer size = 500 Samples

ECG Signal	Huffman Encoding	Delta Encoding	Base-Delta Encoding
Normal	84.9%	73.6%	74.8%
Ventricular Tachycardia	56.1%	0%	43.2%
Ventricular Fibrillation	56.7%	0%	39.1%
Atrial Premature Contraction	53.2%	1.6%	51.7%
Premature Ventricular Contraction	52.4%	1.1%	50.7%
Right Bundle Block	51.7%	0%	55.5%

We found the Huffman encoding technique yields the highest compression ratio over delta and base-delta compression techniques. In contrast, the delta encoding fails to compress abnormal heart conditions. This is due to the uniqueness of each sample in abnormal conditions. On the other hand, the base-delta encoding shows better compression ratios in abnormal heart conditions than the delta encoding technique.

Tables 3.3 and 3.4 summarize the execution time of the compression techniques. We utilize the Real-time Clock (RTC) module on the MCU to calculate the execution time of the three compression techniques. The initial experiment runs the compression techniques in an isolated environment regardless of the other tasks (i.e., the only task running on the MCU).

Table 3.3: Execution time (ms) of lossless encoding algorithms with buffer size = 1000 Samples

ECG Signal	Huffman Encoding	Delta Encoding	Base-Delta Encoding
Normal	112	24	24
Ventricular Tachycardia	112	24	24
Ventricular Fibrillation	112	24	24
Atrial Premature Contraction	112	24	24
Premature Ventricular Contraction	112	24	24
Right Bundle Block	112	24	24

Table 3.4: Execution time (ms) of lossless encoding algorithms with buffer size = 500 Samples

ECG Signal	Huffman Encoding	Delta Encoding	Base-Delta Encoding
Normal	109	23	23
Ventricular Tachycardia	109	23	23
Ventricular Fibrillation	109	23	23
Atrial Premature Contraction	109	23	23
Premature Ventricular Contraction	109	23	23
Right Bundle Block	109	23	23

The Huffman encoding technique shows the highest execution time with a maximum of 112 ms on the buffer size. In contrast, the delta and base-delta techniques show significantly less execution time of a maximum of 24 ms on the same buffer size. From compression ratios and execution time results, we find that the base-delta approach achieves a trade-off between minimum execution time along with a reasonable compression ratio for normal and abnormal cardiac conditions.

3.5.2 Power Consumption Analysis

Based on the data reduction and processing time analysis for each encoding technique, we find the base-delta has promising results. However, we need to evaluate the compression techniques in terms of power consumption to select the best technique that maintains energy saving and extends the ECG patch operational hours.

To evaluate the power consumption for each algorithm, we calculate the required time to transmit the ECG data, captured in 250 and 500 sampling rates, over Bluetooth Low Energy (BLE) at 2 Mbps and 251 bytes payload. Given the total time to transmit one packet over BLE and receive successful delivery acknowledgment is 1.4 ms, the air time to transmit ECG samples over BLE is calculated as follows:

$$\textbf{Air time (ms)} = \frac{\text{Transmitted Data Size}}{251} \times 1.4 \tag{3.3}$$

In Tables 3.5 and 3.6, we present the required transmission time for Huffman, delta and base-delta algorithms in 250 and 500 sampling rates.

Table 3.5: Air time (ms) of the compressed data with buffer size = 500 Samples over BLE at 2 Mbps

ECG Signal	Huffman Encoding	Delta Encoding	Base-Delta Encoding
Normal	2.8	2.9	2.8
Ventricular Tachycardia	7.2	11.1	6.3
Ventricular Fibrillation	7.2	11.1	6.7
Atrial Premature Contraction	7.8	10.9	10.8
Premature Ventricular Contraction	7.9	11	10.9
Right Bundle Block	8	11.1	9.9

Table 3.6: Air time (ms) of the compressed data with buffer size = 1000 Samples over BLE at 2 Mbps

ECG Signal	Huffman Encoding	Delta Encoding	Base-Delta Encoding
Normal	5	6	6
Ventricular Tachycardia	14.66	22.3	12.47
Ventricular Fibrillation	14.4	22.3	13
Atrial Premature Contraction	15.7	21.9	21.5
Premature Ventricular Contraction	15.9	22	22
Right Bundle Block	16	22.3	19.9

We utilize the execution time and air time calculations for each encoding algorithm along with the base current values in Table 3.7 to obtain the power consumption before and after applying the compression task on TI CC2650 MCU as follows:

$$\text{Total Energy} = \text{Air time } (T_{\text{Air}}) * (I_{\text{Tx}} + I_{\text{Core}} + I_{\text{Peri-RF Core}} + I_{\text{Peri-Power Domain}} + I_{\text{Peri-DMA}}) + \text{Processing time } (T_{\text{Proc}}) * (I_{\text{Core}} + I_{\text{Peri-RF Core}} + I_{\text{Peri-Power Domain}} + I_{\text{Peri-DMA}} + I_{\text{Peri-SPI}}) \quad (3.4)$$

Table 3.7: Base power consumption in active power mode

Base Current	Module	Value
I_{Core}	MCU running at 48 MHz	3.39 mA
I_{Peri}	Peripheral Power Domain	97.7 μA
I_{Peri}	Serial Peripheral Interface (SPI)	82.9 μA
I_{Peri}	RF Core idle	210.9 μA
I_{Peri}	μDMA	63.9 μA
I_{Tx}	Radio transmits current 2.4 GHz (BLE)	7.3 mA

In Tables 3.8 and 3.8, We compare Huffman, delta and base-delta performance in terms of the power saving before and after applying data compression. Although Huffman encoding achieves more than 50% as compression ratio in all cardiac conditions, the high execution time affects the overall power consumption. In both sampling rates, the power consumption after applying Huffman exceeds the original power consumption which means Huffman encoding will not produce the optimal energy saving within our constrained embedded environment.

Table 3.8: Power consumption (mJ) on buffer size = 500 Samples while transmitting data over BLE

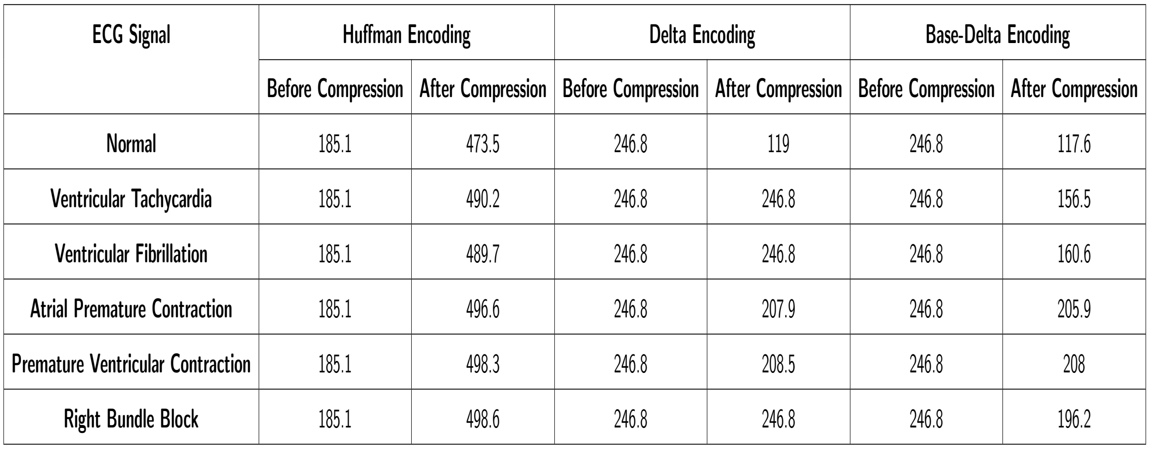

ECG Signal	Huffman Encoding		Delta Encoding		Base-Delta Encoding	
	Before Compression	After Compression	Before Compression	After Compression	Before Compression	After Compression
Normal	185.1	473.5	246.8	119	246.8	117.6
Ventricular Tachycardia	185.1	490.2	246.8	246.8	246.8	156.5
Ventricular Fibrillation	185.1	489.7	246.8	246.8	246.8	160.6
Atrial Premature Contraction	185.1	496.6	246.8	207.9	246.8	205.9
Premature Ventricular Contraction	185.1	498.3	246.8	208.5	246.8	208
Right Bundle Block	185.1	498.6	246.8	246.8	246.8	196.2

Delta encoding achieves 51.7% and 68% power saving in normal ECG using 250 SPS and 500 SPS respectively, and 32% energy saving in atrial premature contraction and premature ventricular contraction. Nonetheless, delta compression fails to preserve power in some cardiac conditions, such as ventricular tachycardia, ventricular fibrillation and right bundle block where the compression ratio is almost zero.

Table 3.9: Power consumption (mJ) on buffer size = 1000 Samples while transmitting data over BLE

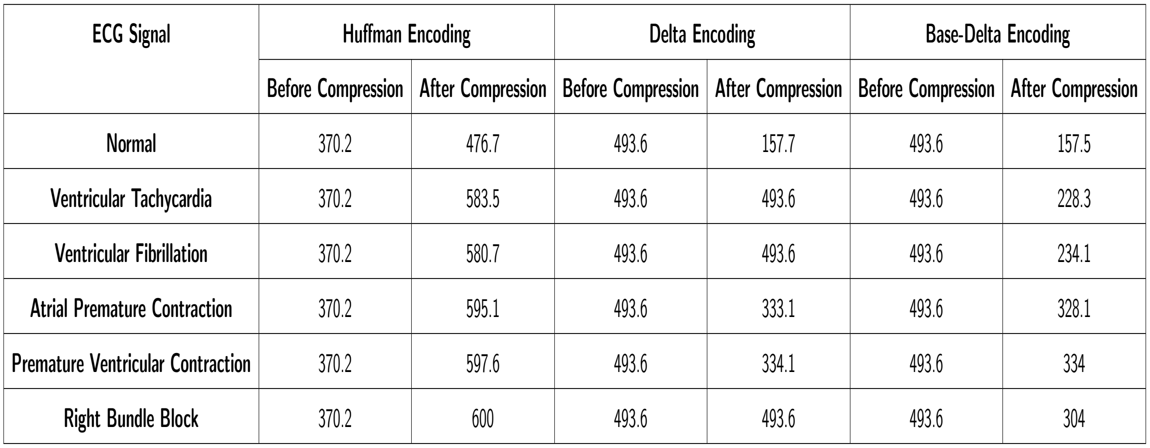

ECG Signal	Huffman Encoding		Delta Encoding		Base-Delta Encoding	
	Before Compression	After Compression	Before Compression	After Compression	Before Compression	After Compression
Normal	370.2	476.7	493.6	157.7	493.6	157.5
Ventricular Tachycardia	370.2	583.5	493.6	493.6	493.6	228.3
Ventricular Fibrillation	370.2	580.7	493.6	493.6	493.6	234.1
Atrial Premature Contraction	370.2	595.1	493.6	333.1	493.6	328.1
Premature Ventricular Contraction	370.2	597.6	493.6	334.1	493.6	334
Right Bundle Block	370.2	600	493.6	493.6	493.6	304

On the other hand, the base-delta algorithm outperforms Huffman and delta encoding and achieves 52.3% and 68% power saving in normal ECG using 250 SPS and 500 SPS respectively. Furthermore, it reaches more than 50% energy saving in ventricular tachycardia and ventricular fibrillation besides 30 % power saving in atrial premature contraction, premature ventricular contraction and right bundle block conditions.

3.6 Summary

To conclude, the base-delta encoding fulfills our ECG data acquisition hardware constraints. It makes a trade-off between the required stringent execution time and the compression ratio while extending the battery life of the ECG patch.

Chapter 4

Adaptive ECG Leads Selection

4.1 Motivation

Based on the medical literature, cardiovascular risks could be categorized into: arrhythmias [96] [97], myocardial infarction [98] [99], heart blocks [100] [101]. The ECG abnormalities could be diagnosed using various ECG leads based on the cardiovascular risk category. In this chapter, we consider the adaptive selection of ECG leads as a second approach for reducing the required number of transmitted ECG channels, and evaluating the effect on the power consumption of the ECG patch within the constrained embedded environment. We will demonstrate the effect of minimizing the number of ECG leads on the battery life of the MCU after applying ECG classification techniques, such as binary and multi-class classification, which act as intelligent decision makers to control the streamed channels. Furthermore, we will compare the air time to transmit ECG data and the energy saving in binary and multi-class classification scenarios concerning the TI CC2650 MCU environment.

4.2 Binary Classification

In a constrained real-time monitoring platform, we need to balance the processing time of ECG classification and accuracy for abnormalities detection. Saenz-Cogollo et al. [102] introduce a novel features selection technique using a filter method based on the mutual information ranking criterion on the training set. The authors recommend that both normalized beat-to-beat (R–R) intervals and QRS complexes are the most distinct features for cardiac disease diagnosis. Badr et al. [103] utilize the novel features selection technique to present an intensive comparison between distinct ML algorithms regarding accuracy and execution time for ECG anomaly detection.

4.2.1 Methodology

To distinguish the normal and abnormal ECG signals, we reproduce the experimental results in both studies [102] [103] with the popular supervised learning algorithms, such as Random Forest (RF), Support Vector Machine (SVM), K-Nearest Neighbor (KNN), and Logistic Regression (LR). Signals were extracted from the original files of the MIT-BIH database using the native Python waveform database (WFDB) and re-sampled at 500 Hz to simulate the same sampling rate as our ECG patch.

4.2.2 Datasets

We use the MIT-BIH arrhythmia database [104] which contains 48 ECG recordings for 47 patients. Each record contains 30 minutes of ECG readings collected from 47 subjects by the BIH Arrhythmia Laboratory between 1975 and 1979. The recordings were digitized at 360 samples per second per channel with 11-bit resolution over a

10 mV range. Two or more cardiologists independently annotated each record to obtain the computer-readable reference annotations for each heartbeat (approximately 110,000 annotations). According to the work introduced in [77], the dataset includes 15 types of ECG arrhythmia. We choose the most common abnormalities, premature ventricular contraction (PVC), paced beat (PAB), right bundle branch block beat (RBBB), left bundle branch block beat (LBBB), atrial premature contraction (APC), ventricular flutter wave (VFW), and ventricular escape beat (VEB). In addition, we use the normal annotated records to get a balanced dataset with normal and abnormal cases. We divide the dataset into 22 records for the training set and 22 records for the testing set as shown in Table 4.1 and Table 4.2.

Table 4.1: Training set with MIT-BIH annotated records

ECG Class	**Annotated Records**
Normal	101, 108, 112, 114, 115, 122
PVC	106, 116, 119, 201, 203, 208
PAB	102, 217
RBBB	118, 124
LBBB	109, 213
APC	209, 220,223
VFW	207
VEB	207

Table 4.2: Testing Set with MIT-BIH annotated records

ECG Class	Annotated Records
Normal	100, 103, 105, 113, 117, 121, 123, 202
PVC	200, 210, 221, 228, 233
PAB	104, 107
RBBB	212, 231
LBBB	111, 213
APC	222, 232
VFW	207
VEB	207

4.2.3 Features Extraction

The original study in [102] considers a total of 85 features which are divided into beat-to-beat (R–R) intervals, discrete wavelet transform (DWT) coefficients, Hermite basis function (HBF) expansion coefficients, higher-order statistics (HOS), amplitude differences, Euclidean distances and temporal characteristics of the ventricular depolarization waves (QRS complex). Doquire et al. [105] propose mutual information (MI) ranking criterion, We use the same criteria on the training set to rank the most informative features relative to the heartbeat type classes. Table 4.3 shows the top 10 ranked features we obtain from the mutual information (MI) ranking criterion.

Table 4.3: Top 10 features as ranked by the MI criterion for the reference annotations of the MIT-BIH database

Rank	Feature	Description
1	hbf_2	The coefficients of fitting Hermite basis functions with polynomials degree = 2
2	hbf_3	The coefficients of fitting Hermite basis functions with polynomials degree = 3
3	hbf_12	The coefficients of fitting Hermite basis functions with polynomials degree = 12
4	hbf_1	The coefficients of fitting Hermite basis functions with polynomials degree = 1
5	RR0/avgRR	The current R-R interval divided by the average of the last 32 beats
6	RR+1/RR0	The following R-R interval divided by the current R-R interval
7	hbf_11	The coefficients of fitting Hermite basis functions with polynomials degree = 11
8	QRSw4_norm	The normalized QRS complex at a quarter of the peak value
9	RR-1/RR0	The previous R-R interval divided by the average of the last 32 beats
10	hbf_10	The coefficients of fitting Hermite basis functions with polynomials degree = 10

4.2.4 Supervised Learning Results

We train the MIT-BIH arrhythmia database on RF, SVM, KNN, and LR models to compare them in terms of accuracy, execution time, precision, recall, and F1 score. In Table 4.4, LR outperforms the other algorithms in the total processing time with 0.857 Sec, while RF achieves the highest accuracy score with 94.8%

Table 4.4: Execution time and accuracy of binary classification algorithms

	LR	RF	SVM	KNN
Execution Time (Sec)	0.857	52	306	8.3
Accuracy (%)	93.5	94.8	94.2	94

We verify the accuracy scores by visualizing the cross-validation versus the training scores for each classification model. Figure 4.1, Figure 4.2, Figure 4.3, and Figure 4.4

represent the performance of LR, RF, SVM, and KNN classifiers, respectively.

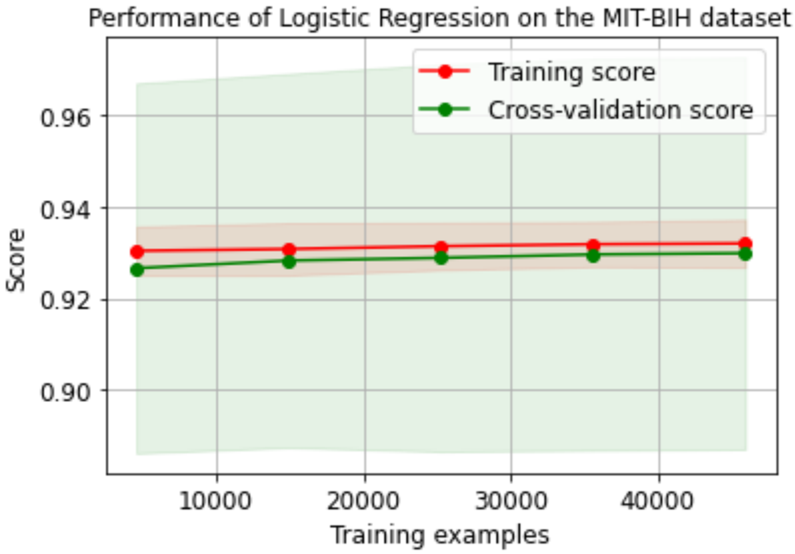

Figure 4.1: Cross validation score vs training score for the LR classifier

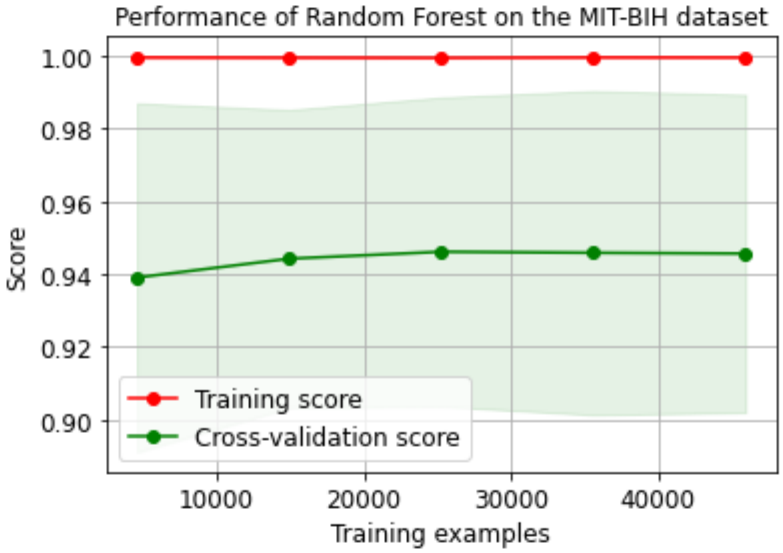

Figure 4.2: Cross validation score vs training score for the RF classifier

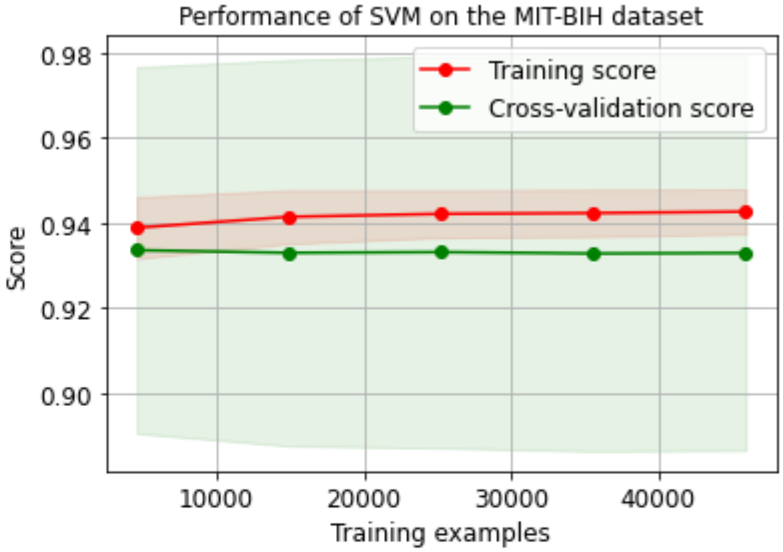

Figure 4.3: Cross validation score vs training score for the SVM classifier

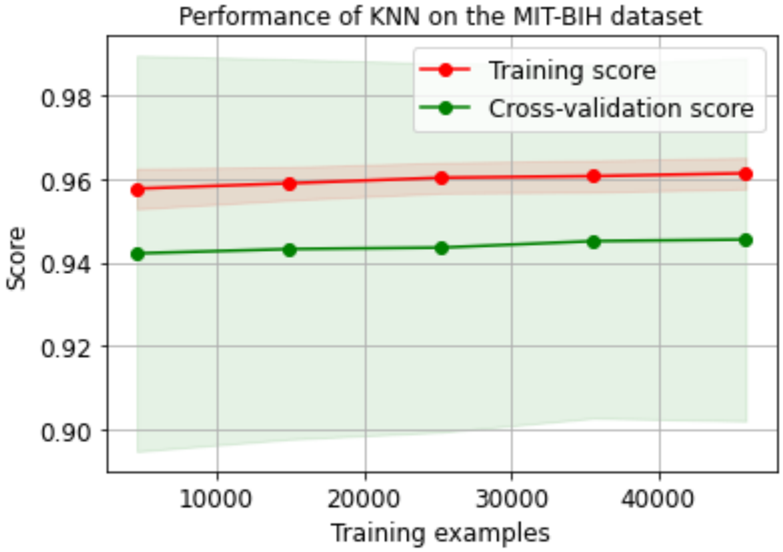

Figure 4.4: Cross validation score vs training score for the KNN classifier

In Table 4.5, we evaluate LR, RF, SVM, and KNN based on the precision, recall, and F1-score values in normal and abnormal ECG signals. The KNN classifier achieves the maximum precision in the normal ECG, and the SVM has the highest precision in abnormal conditions. For the recall scores, the SVM classifier is at the top in the normal case despite KNN being the maximum in the abnormal case. The RF classifier obtains the highest F1-score for both normal and abnormal classes. We found that the results of the normal ECG class significantly exceed the abnormal class due to the imbalanced MIT-BIH database where the number of normal recordings is two times the abnormal recordings. A potential solution to this problem is perform data augmentation and regularization to overcome the limitations of dataset size and data variation. However, this is beyond the scope of this work.

Table 4.5: Evaluation report for binary classification algorithms in normal and abnormal ECG

		LR	**RF**	**SVM**	**KNN**
Normal Class	**Precision**	94.7%	96.1%	95.2%	96.8%
	Recall	98.2%	98.1%	98..3%	96.5%
	F1-Score	96.4%	97.1%	96.8%	96.6%
Abnormal Class	**Precision**	79.3%	82%	82.1%	72.5%
	Recall	55.9%	67.9%	60.3%	74.1%
	F1-Score	65.5%	74.3%	69.5%	73.3%

According to the constraints of the embedded environment on computational time, We found that the LR model satisfies our ECG platform requirements in terms of accurate diagnosis and minimum computational complexity with 93.60% accuracy and 0.857 Sec processing time. The binary classification will act as an intelligent decision-maker to control the ECG patch's mode of operation based on the current ECG readings. By controlling the mode of operation on the ECG patch, we can reduce the number of required ECG leads and thus reduce the total energy consumption required for data transmission.

4.2.5 System Flow in Binary Classification Scenario

The system design includes multiple stages as shown in Figure 4.5. We train the LR model offline using the annotated ECG recordings of the MIT-BIH arrhythmia database. The classifier then classifies the ECG readings acquired by the ECG patch into normal and abnormal classes. The ECG patch runs the 12-leads streaming mode by default to enable full-scale ECG analysis. Our proposed power-saving approach is to let the ECG patch stream only a single lead by default and switch to more leads when abnormal conditions are detected. Energy-saving would be feasible due to data size reduction between the 12-lead mode which generates 27648 bytes during 2 Sec, and the single lead mode which generates 6144 bytes in 2 Sec.

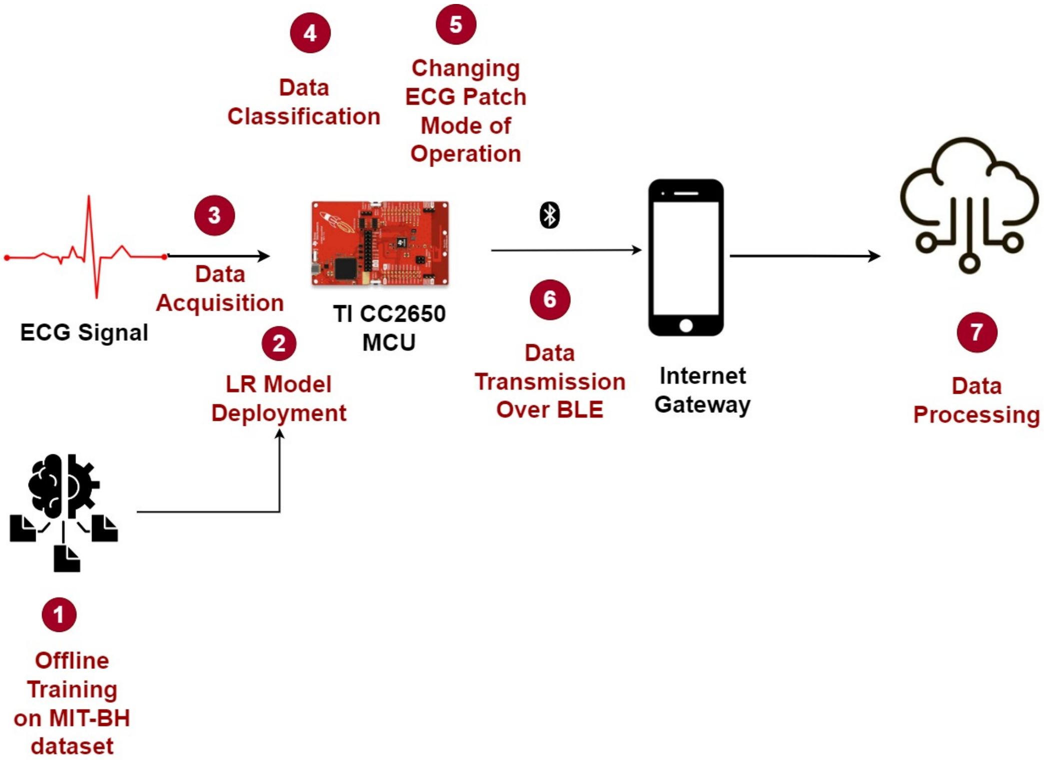

Figure 4.5: Energy saving scenario using varying modes of operations

4.2.6 Power Consumption Analysis Using Binary Classification

To maintain the ECG system availability, we must minimize the total power consumed in the acquisition and transmission stages. Energy-saving scenario using the binary classification is assessed and compared with the original scenario (i.e., Single lead data transmission) in respect of the air time to transmit the ECG data, the total power consumption, and the amount of saved energy.

The required duration to capture at least one full R-R signal equals 2 Sec. Our ECG patch operates on a 500 sampling rate. So, we need 1000 samples to detect a complete cardiac cycle. We calculate the required air time given 251 bytes payload, and 1.4 ms to transmit the data packet and get acknowledgment after the successful delivery according to the following equation:

$$\text{Air time to transmit ECG data} = \frac{\text{Size of transmitted ECG data}}{251} * 1.4 \tag{4.1}$$

Table 4.6 compares the 1 lead ECG streaming scenario in the original and LR states in terms of the required air time while transmitting the ECG data to the internet gateway over BLE with 2 MBPS physical layers and 251 bytes payload. For the binary classification scenario, we consider the air time in the single lead mode for normal ECG. Next, we evaluate the air time for 12 leads (8 channels) mode in the abnormal cases. As shown in Table 4.6, the normal ECG in the classification approach has air time less than the original state. On the other hand, the binary classification scenario has the maximum air time when we switch to the 12-lead mode.

Table 4.6: Air time (ms) before and after binary classification

ECG Signal	Original Scenario	LR Scenario
Normal	45	34.2
PVC	45	154.2
PAB	45	154.2
RBBB	45	154.2
LBBB	45	154.2
APC	45	154.2
VFW	45	154.2
VEB	45	154.2

After air time calculations, we evaluate the total power consumption in the normal ECG condition (i.e., single lead mode of operation), and the ECG abnormal condition (i.e., 12-lead mode of operation). The comparability of power consumption after using the binary classification technique to control the patch mode of operation from 12 leads to a single lead highlights that power consumption can be reduced in the normal condition only, as shown in Table 4.7, with a 77.7% power saving.

Table 4.7: Power consumption (mJ) for 12 leads before and after classification

ECG Signal	Original Scenario	LR Scenario
Normal	1706	379.1
PVC	1706	1706
PAB	1706	1706
RBBB	1706	1706
LBBB	1706	1706
APC	1706	1706
VFW	1706	1706
VEB	1706	1706

4.2.7 Merging Binary Classification with Base-Delta Compression

To study the effect of combining the binary classification and base-delta compression on the power saving, we start with classifying the captured ECG signal using the LR model as mentioned previously. Afterwards, we change the ECG patch mode of operation between 1 and 12 leads based on the classification results either normal or abnormal and compress the data with base-delta before transmission over BLE.

Table 4.8 summarizes the power-saving for the compression scenario on 12 leads and compression after classification. To obtain the power-saving readings, we calculate both the processing time and air time for each ECG condition concerning the base current of the TI CC2650 MCU using the following formula (where the I's are the active modules from the board data sheet) [106]:

$$\text{Total Energy} = \text{Air time } (T_{\text{Air}}) * (I_{\text{Tx}} + I_{\text{Core}} + I_{\text{Peri-RF Core}} + I_{\text{Peri-Power Domain}} + I_{\text{Peri-DMA}}) + \text{Processing time } (T_{\text{Proc}}) * (I_{\text{Core}} + I_{\text{Peri-RF Core}} + I_{\text{Peri-Power Domain}} + I_{\text{Peri-DMA}} + I_{\text{Peri-SPI}}) \tag{4.2}$$

According to the results, applying base-delta compression after the LR classification has power-saving ratios close to the results of using compression only. However, the computational overhead will increase as we need to execute the binary classification before compressing the captured ECG signals.

Table 4.8: Energy saving in compression and classification scenarios

ECG Signal	**Compression Scenario**	**LR & Compression Scenario**
Normal	41.2%	33.5%
PVC	33.4%	30.9%
PAB	34.7%	31.2%
RBBB	33.8%	36.8%
LBBB	32.6%	31.3%
APC	41.9%	33%
VFW	33.4%	32.8%
VEB	33.6%	33%

4.3 Multi-Class Classification

In light of the promising results of energy saving in the binary classification approach [107], we investigate the possibility of changing the number of required ECG leads to diagnose specific cardiac abnormalities using multi-class classification. The alteration of the ECG patch mode of operation (i.e., changing the number of ECG channels) will affect the total power needed to transmit the ECG data over BLE to the internet gateway device. In this section, we will compare the popular existing deep learning models that work on single lead or 12 leads to classify irregular cardiovascular rhythms, and discuss the impact of applying these models on the total energy saving of our real-time ECG platform.

4.3.1 Multi-Class Classification Using a Single ECG Lead

Hannun et al. [108] introduce a cardiologist-level arrhythmia detection to classify 12 rhythm classes using a single lead ambulatory ECG. The authors aim to classify a wide range of distinct arrhythmias with high diagnostic performance similar to the level of ECG evaluation from expert cardiologists. Our proposed scenario is to operate the ECG patch on the single lead as a default operation mode. Figure 4.6 shows the system flow in the multi-classification scenario where the streamed data from the single lead will be classified using the neural network model. Based on the detected ECG class, we will change the number of streamed ECG channels to ensure accurate ECG readings. The ECG patch operation mode would reset to single lead mode after 30 minutes of streaming the required channels.

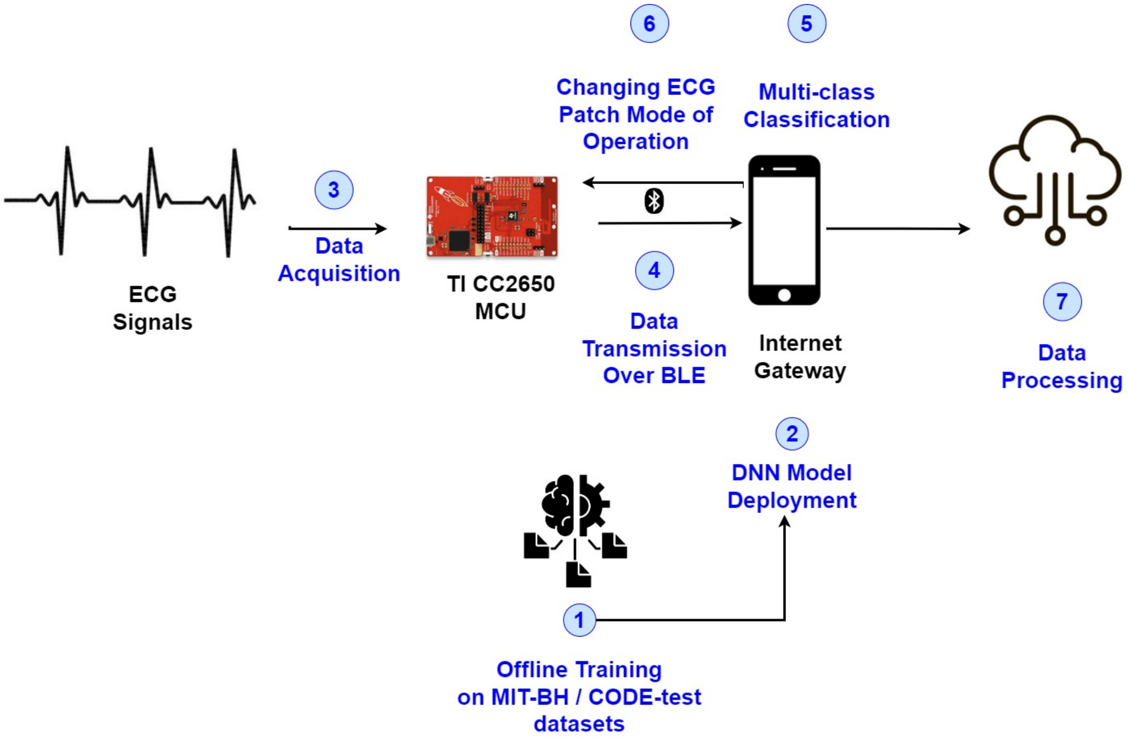
6
Changing ECG Patch Mode of Operation
5
Multi-class Classification
ECG Signals
3
Data Acquisition
TI CC2650 MCU
4
Data Transmission Over BLE
Internet Gateway
7
Data Processing
2
DNN Model Deployment
1
Offline Training on MIT-BH / CODE-test datasets

Figure 4.6: System flow using the multi-class classification approach

4.3.1.1 Dataset

The authors in [108] collect a large, novel ECG rhythm dataset which is annotated by a group of cardiologists [109] and contains 10 arrhythmias, such as Atrioventricular Block (AVB), Atrial Fibrillation, Ventricular tachycardia, Bigeminy, Trigeminy, Junctional Rhythm, Idioventricular Rhythm (IVR), Ecoptic Atrial Rhythm (EAR), Wenckebach, Supraventricular Tachycardia (SVT) as well as sinus rhythm and noise. The rhythm dataset consists of 91,232 ECG records from 53,549 patients.

The ECG records are captured using Zio monitor [110], an ambulatory cutaneous single lead ECG monitoring device, that continuously records data from Lead II at 200 Hz. The test dataset contains 328 ECG records collected from 328 unique patients, which is also annotated by a committee of expert cardiologists.

4.3.1.2 Deep Neural Network Architecture

Hannun et al. propose a Deep Neural Network (DNN) which accepts ECG raw signal sampled at 200 Hz as input for the 1st convolutional layer as shown in Figure 4.7. The DNN contains 33 convolutional layers total followed by a linear output layer to one of 12 rhythm classes. Additionally, 16 residual blocks act as short connections for fast back-propagation. The batch normalization and rectified linear activation unit (ReLU) activation function are used to control the vanishing gradients. Furthermore, max pooling is applied to reduce the dimensionality of data features, and eliminate data over-fitting. The dense layer is used for changing the dimensions of the neurons vector and the output of the dense layer will be the input of the softmax activation function that produces a vector to represent the probability distributions of the 12 rhythm classes.

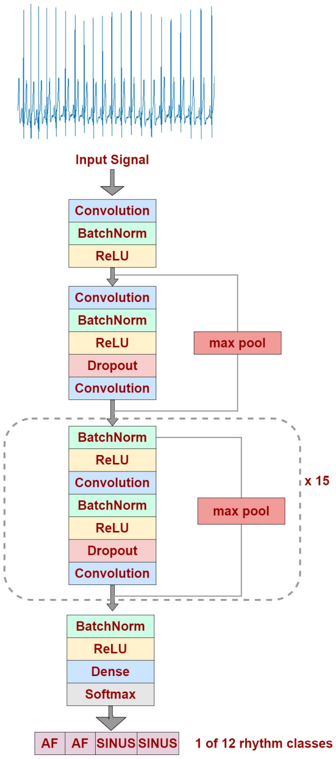

Figure 4.7: DNN architecture using single lead (Adapted from [108])

4.3.1.3 Methodology

We target deploying the DNN introduced by Hannun et al. [108] using the MIT-BIH arrhythmia database to assure the diversity of cardiac risks between arrhythmias and heart blocks. The training was applied offline before model deployment on the gateway device. We select 80:20 as a ratio between the training set and the testing set. The multi-class classification with the MIT-BIH arrhythmia database produces seven cardiac classes as shown in Table 4.9.

Table 4.9: Multi-class classification output classes using MIT-BIH arrhythmia database

ECG Annotation	Class
N	Normal Beat
V	Premature Ventricular Contraction
L	Left Bundle Branch Block Beat
R	Right Bundle Branch Block Beat
/	Paced Beat
S	Supraventricular premature
A	Atrial premature beat

We utilize the DNN architecture and initialize the Adam optimizer with the parameters described in Table 4.10.

Table 4.10: Hyper-parameters tuning with Adam optimizer

Hyper-Parameter	Value
$\beta1$	0.9
$\beta2$	0.999
Learning Rate	0.001
Batch Size	128 Samples

4.3.1.4 Multi-Class Classification Evaluation

After training and testing the single lead DNN model on the MIT-BIH arrhythmia database, we found that the DNN model achieves 99% accuracy to classify the raw ECG signals into seven different classes. To obtain valuable insights about the DNN predictions, we visualize the true positives, true negatives, false positives, and false negatives using the confusion matrix as shown in Figure 4.8

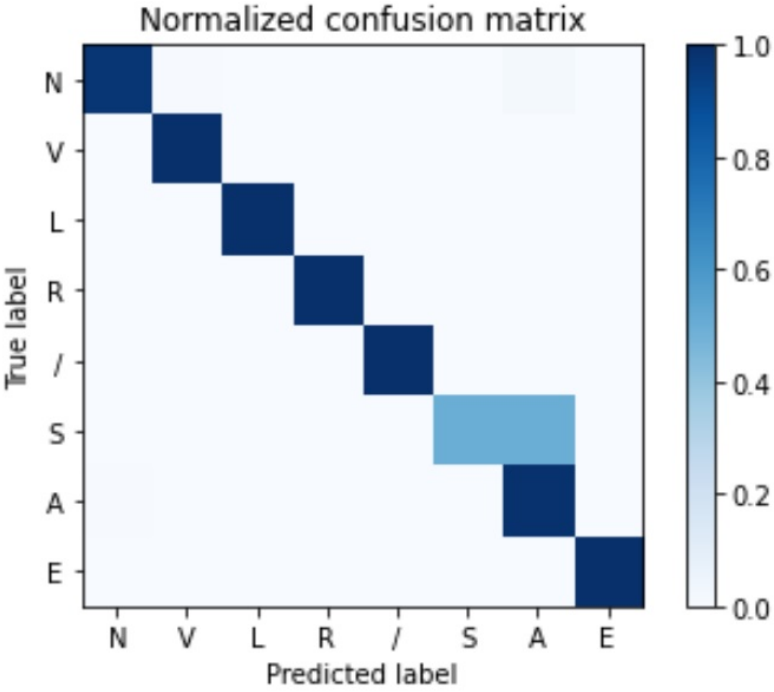

Figure 4.8: Confusion matrix of the single lead DNN model

In Table 4.11, we evaluate the single lead DNN model in terms of precision, recall, and F1-score for each ECG class. Results show that both types of heart blocks and paced beats have the maximum precision, recall, and F1-scores. On the other hand, the Supraventricular premature class has the minimum recall, and F1-score values.

Table 4.11: Evaluation report for multi-class classification with MIT-BIH arrhythmia database

	Precision	**Recall**	**F1-Score**
N	0.99	0.98	0.98
V	1.00	0.99	0.99
L	1.00	1.00	1.00
R	1.00	1.00	1.00
/	1.00	1.00	1.00
S	1.00	0.5	0.67
A	0.83	0.99	0.90

4.3.1.5 Power Consumption Analysis

In this scenario, the number of required ECG leads varies between 1, 4, and 12 based on the detected ECG class. For instance, the normal and paced classes will only need one lead. Both right and left bundle heart blocks need four leads (V1, V2, V5, V6) to be diagnosed [111][112] while the premature ventricular contraction, the Supraventricular premature, and the atrial premature beat will need 12 leads for efficient medical evaluation.

The commercial ECG monitoring devices are released with a different number of channels between 1 and 8 channels where 1 channel could be represented by a single lead, 3 channels are represented with 3 or 4 leads, and 8 ECG channels mean 12 leads. Given 24 bits of data for each channel, and 24 bits for channel status, the data size produced by **(N)** ECG channels and total data size at 500 sampling rate can be calculated as follows:

$$\text{Data Size of } \mathbf{(N)} \text{ Channels (Bits)} = \text{N} * \text{Channel Data Bits} + \text{Channel Status Bits} \tag{4.3}$$

$$\text{Data Size at 500 Sampling Rate (Bytes)} = \frac{500 * \text{Data Size for } \mathbf{(N)} \text{ Channels}}{8} \tag{4.4}$$

Table 4.12 shows the number of ECG channels needed for each cardiac class resulting from the single lead DNN and the total data size streamed from these channels at a 500 sampling rate.

Table 4.12: ECG channels for each cardiac class of the single lead DNN

ECG Class	# of Required Leads	# of Required Channels	Data Size for (N) Channels (Bits)	Data Size at 500 Sampling Rate (kB)
N	1	1	48	3
V	12	8	216	13.5
L	4	3	96	6
R	4	3	96	6
/	1	1	48	3
S	12	8	216	13.5
A	12	8	216	13.5

Power consumption measurements are calculated using equations (4.1) and (4.2) given 500 samples/Sec as a sampling rate and a minimum 2 Sec duration to capture the full cardiac cycle.

Energy saving is achieved by changing the mode of operation for the ECG patch based on the detected ECG class and eliminating the need of streaming the 12 ECG leads continuously which drains the patch battery. In Table 4.13, we demonstrate the power consumption before (i.e., 12-lead streaming) and after (i.e., streaming with a varied number of leads) the multi-class classification. We reach the maximum energy saving in single lead and 4 lead scenarios with 77.7% and 55.5% respectively.

Table 4.13: Power consumption and energy saving after using single lead DNN

ECG Class	Power Consumption Using 12 Leads (mJ)	Power Consumption Using Adaptive Leads Selection (mJ)	Power Saving (%)
N	1706	379.1	77.7
V	1706	1706	-
L	1706	758.2	55.5
R	1706	758.2	55.5
/	1706	397.1	77.7
S	1706	1706	-
A	1706	1706	-

4.3.2 Multi-class Classification Using 12 ECG Leads

To validate the energy saving using a multi-class classification approach, we need to examine the output resulting from different conditions, such as the used DNN models or the diversity of ECG datasets. In the previous section, we evaluated the power consumption using the open source single lead DNN model provided by Hannun et al. [108], and it was energy-efficient. However, we found the power consumption evaluation is still largely unexplored for the constrained environments using 12-lead datasets with DNN models. Ribeiro et al. [113] highlight the shortage of 12-lead digital ECG datasets with systematic annotation of the full list of ECG diagnosis. They build a large-scale labelled dataset and deploy a DNN model to classify six ECG abnormalities. We will deploy the open-source DNN model proposed by Ribeiro et al. to measure the impact of their classifier on the ECG patch power consumption.

4.3.2.1 Dataset

The authors in [113] create a large annotated ECG dataset called CODE-test [114] that contains 2,322,513 ECG records from 1,676,384 different patients of 811 counties in the state of Minas Gerais/Brazil. Ribeiro et al. release 827 ECG tracings from the total dataset records for public usage. All the records are annotated by cardiologists, residents, and medical students. The CODE-test dataset includes six different rhythmic and morphologic ECG abnormalities.

4.3.2.2 Deep Neural Network Architecture

Ribeiro et al. [113] propose a Deep Neural Network (DNN) based on the previous work of Hannun et al. [108] with fewer convolutional layers. The modified DNN accepts ECG raw signal sampled at 400 Hz as an input (i.e., 4096 samples / each lead in 10-sec duration) for the 1st convolutional layer followed by four residual blocks as shown in Figure 4.9. Each residual block has two convolutional layers where the batch normalization is applied to the output of each convolutional layer before being parsed to the ReLU activation function. The convolutional layers have 64 filters with a length of 16 for the first convolutional layer and residual block and increasing the number of filters by 64 every second residual block. The output of the last residual block is an input for the dense layer with a Sigmoid activation function as some records have intersected classes. Both max Pooling and (1x1 Conv) are used in the skip connections to guarantee the dimensions match between the skip connection and the signals in the main network flow.

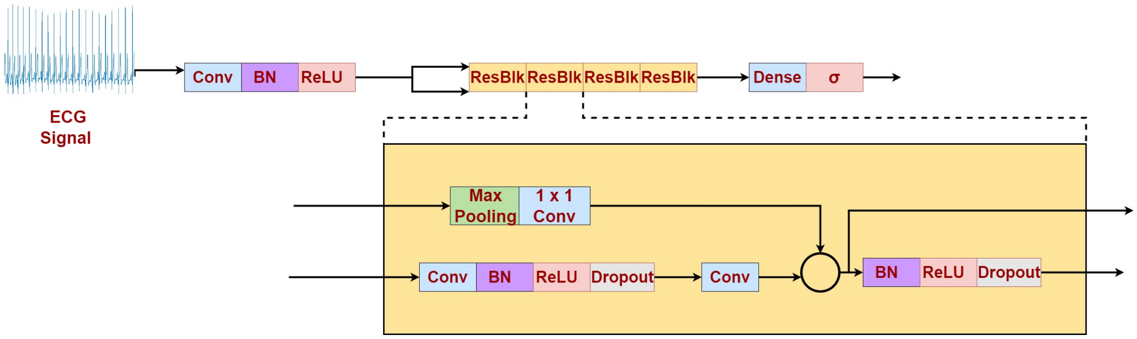

Figure 4.9: DNN architecture using 12 leads (Adapted from [113])

4.3.2.3 Methodology

We use the DNN architecture introduced by Ribeiro et al. [113] using the CODE-test dataset to evaluate the power consumption with a different set of cardiac irregularities. As mentioned earlier, the training was applied offline before model deployment on the gateway device. We select 80:20 as a ratio between the training set and the testing set. The multi-class classification with the CODE-test dataset produces six cardiac classes as shown in Table 4.14.

Table 4.14: Multi-class classification output classes using CODE-test dataset

ECG Annotation	**Class**
1dAVb	1st Degree AV Block
SB	Sinus Bradycardia
LBBB	Left Bundle Branch Block Beat
RBBB	Right Bundle Branch Block Beat
AF	Atrial Fibrillation
ST	Sinus Tachycardia

We implemented the DNN architecture [113], and initialized Adam optimizer with the parameters described in Table 4.15.

Table 4.15: Hyper-parameters tuning with Adam optimizer

Hyper-Parameter	Value
$\beta1$	0.9
$\beta2$	0.999
Learning Rate	0.001
Batch Size	64 Samples

4.3.2.4 Mutli-Class Classification Evaluation

After training and testing the 12 lead DNN model on the CODE-test dataset, we found that the DNN model achieves 99.5% accuracy to classify the raw ECG signals into five different classes We visualize the true positives, true negatives, false positives, and false negatives using the confusion matrix as shown in Figure 4.10 to obtain insights about the DNN predictions.

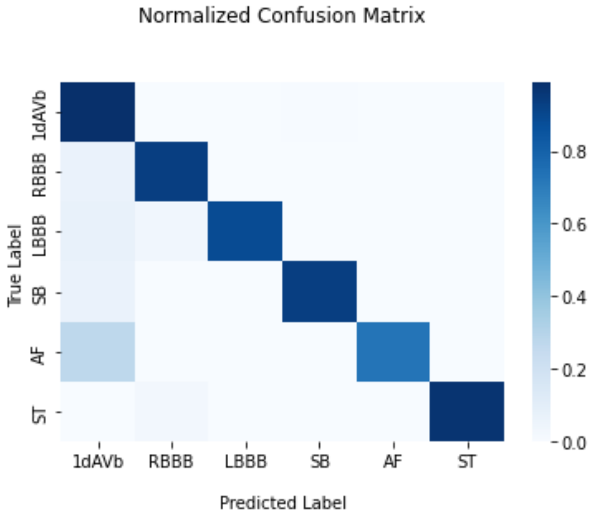

Figure 4.10: Confusion matrix of the 12-lead DNN model

In Table 4.16, We evaluate the 12-lead DNN model in terms of precision, recall, and F1-score for each ECG class. The resultant scores from the reproducible implementation and the paper results are the same. The left bundle block and atrial fibrillation classes have the maximum precision scores. The left and right heart blocks classes achieve the highest recall scores while the left bundle and sinus tachycardia have the best F1 scores.

Table 4.16: Evaluation report for multi-class classification with CODE-test dataset

	Precision	**Recall**	**F1-Score**
1dAVb	0.86	0.92	0.89
RBBB	0.89	1.00	0.94
LBBB	1.00	1.00	1.00
SB	0.833	0.93	0.88
AF	1.00	0.76	0.87
ST	0.94	0.97	0.96

4.3.2.5 Power Consumption Analysis

In this scenario, the number of required ECG leads varies between 3, 4, and 12 leads for the abnormal ECG signals and 1 lead for the normal condition. As an example, sinus bradycardia needs 3 leads (II, III and aVF) to be diagnosed [115] while sinus tachycardia requires 4 leads (V3, V4, V5, V6) for the accurate medical evaluation [116]. Furthermore, both right and left bundle heart blocks need 4 leads (V1, V2, V5, V6) to be diagnosed [111][112]. The 1dAVB and the atrial fibrillation are under the arrhythmias category where 12 leads are crucial to maintain an effective diagnosis.

Table 4.17 shows the number of ECG channels needed for each cardiac class resulting from the 12 leads DNN, and the total data size streamed from these channels at a 500 sampling rate using equations (4.3) and (4.4) on each ECG class.

Table 4.17: ECG channels for each cardiac class of the 12 lead DNN

ECG Class	# of Required Leads	# of Required Channels	Data Size for (N) Channels (Bits)	Data Size at 500 Sampling Rate (kB)
1dAVB	12	8	216	13.5
RBBB	4	3	96	6
LBBB	4	3	96	6
SB	3	3	96	6
AF	12	8	216	13.5
ST	4	3	96	6

Similarly to the single lead DNN, the power consumption measurements are calculated using equations (4.1) and (4.2) with a 500 sampling rate and a minimum 2 Sec duration to capture the full cardiac cycle. In Table 4.18, we demonstrate the power consumption before and after applying the multi-class classification. As a result, we get the maximum energy saving in 3 and 4 leads scenarios with 55.5%.

Table 4.18: Power consumption and energy saving after using 12-lead DNN

ECG Class	Power Consumption Using 12 Leads (mJ)	Power Consumption Using Adaptive Leads Selection (mJ)	Power Saving (%)
1dAVB	1706	1706	-
RBBB	1706	758.2	55.5
LBBB	1706	758.2	55.5
SB	1706	758.2	55.5
AF	1706	1706	-
ST	1706	758.2	55.5

4.4 Summary

In this chapter, we investigate the effect of binary and multi-class classification on the ECG patch power consumption. In the binary classification approach, we found LR achieves 77.7% regarding the power saving for the normal conditions, when the mode of operation is changed from 12 leads to one lead. We introduce the adaptive ECG leads selection by applying multi-class classification with CNN on the MIT-BIH and CODE-test datasets. The adaptive leads selection technique saves 77.7% of the total power consumption in the normal ECG status compared to 55.5% energy saving in the abnormal ECG conditions.

Chapter 5

Conclusion and Future Work

5.1 Conclusion

In this work, we investigate distinct procedures to support continuous cardiac event monitoring within the constrained embedded environment of TI-CC2650 MCU. We study the impact of data compression, and adaptive selection of ECG leads on energy saving. The Huffman, delta, and base-delta encoding algorithms are evaluated regarding the compression ratio, execution time, and energy consumption for data transmission. The base-delta encoding outperformed the Huffman and delta encoding techniques and achieved a 24 ms execution time, a 70% compression ratio in normal cardiac status, and more than 40% in abnormal cardiac status. In addition, the delta encoding technique saved 50% of the power consumption compared to no compression.

We evaluate the effect of applying binary classification to switch the ECG patch mode of operation in terms of execution time, airtime over BLE, and energy-saving ratios. Changing the mode of operation approach exceeds base-delta in terms of energy saving of 77.7% for the normal conditions only when the mode of operation is changed from 12 leads to 1 lead. Nonetheless, base-delta encoding shows a stable power saving of 41.2% in normal ECG and 33% in abnormal status. Additionally, base-delta meets the embedded environment constraints with 25 ms execution time and 20 ms transmission time compared to 857 ms and 154 ms in the binary classification with Logistic Regression. We provide a flexible choice of ECG channels based on the cardiac classification output from two varied CNN models that are deployed on single-lead and 12-leads datasets. Based on the detected cardiac class, we change the ECG patch mode of operation, extending the battery life and preserving continuous ECG evaluation. The adaptive leads selection technique saves 77.7 % of the total power consumption in the normal ECG status compared to 55.5 % energy saving in the abnormal ECG conditions.

5.2 Future Work

The datasets used in the literature have a few limitations, such as the limited number of leads, the small number of cardiac cases, or the unbalance recordings (i.e., the number of normal recordings exceeds the abnormal recordings). It will be important that future work considers creating an intensive dataset with a wide diversity of cardiac abnormalities to overcome these limitations. Future studies could also examine the effect of using hybrid compression techniques on the input of CNN models and compare the performance of the ECG real-time platform and the total energy saving before and after applying these techniques. Furthermore, we plan to apply the adaptive ECG channel selection as a bench-marking approach using datasets with a broader range of cardiovascular diseases to expand the operational hours of the low-powered ECG diagnosis platforms.

Bibliography

[1] G. A. Roth, D. Abate, K. H. Abate, S. M. Abay, C. Abbafati *et al.*, “Global, regional, and national age-sex-specific mortality for 282 causes of death in 195 countries and territories, 1980–2017: A systematic analysis for the global burden of disease study 2017,” *The Lancet*, 2018.

[2] (2020) World health organization, the top 10 causes of death, https://www.who.int/news-room/fact-sheets/detail/the-top-10-causes-of-death.

[3] S. Selvaraj and S. Sundaravaradhan, “Challenges and opportunities in IoT healthcare systems: A systematic review,” *SN Applied Sciences*, vol. 2, no. 1, pp. 1–8, 2020.

[4] M. N. Birje and S. S. Hanji, “Internet of things based distributed healthcare systems: A review,” *Journal of Data, Information and Management*, vol. 2, no. 3, pp. 149–165, 2020.

[5] C. Beach, S. Krachunov, J. Pope, X. Fafoutis, R. J. Piechocki, I. Craddock, and A. J. Casson, “An ultra low power personalizable wrist worn ecg monitor integrated with iot infrastructure,” *IEEE Access*, vol. 6, pp. 44 010–44 021, 2018.

[6] M. A. Serhani, H. T. El Kassabi, H. Ismail, and A. Nujum Navaz, "ECG monitoring systems: Review, architecture, processes, and key challenges," *Sensors*, vol. 20, no. 6, p. 1796, 2020.

[7] N. Faruk, A. Abdulkarim, I. Emmanuel, Y. Y. Folawiyo, K. S. Adewole, H. A. Mojeed, A. A. Oloyede, L. A. Olawoyin, I. A. Sikiru, M. Nehemiah *et al.*, "A comprehensive survey on low-cost ECG acquisition systems: Advances on design specifications, challenges and future direction," *Biocybernetics and Biomedical Engineering*, 2021.

[8] G. Hinton, "Deep learning—a technology with the potential to transform health care," *Jama*, 2018.

[9] T. Tekeste, H. Saleh, B. Mohammad, and M. Ismail, "Ultra-low power QRS detection and ECG compression architecture for IoT healthcare devices," *IEEE Transactions on Circuits and Systems I: Regular Papers*, vol. 66, no. 2, pp. 669–679, 2018.

[10] J. Hoffmann, S. Mahmood, P. S. Fogou, N. George, S. Raha, S. Safi, K. J. Schmailzl, M. Brandalero, and M. Hübner, "A survey on machine learning approaches to ECG processing," in *2020 Signal Processing: Algorithms, Architectures, Arrangements, and Applications (SPA)*. IEEE, 2020, pp. 36–41.

[11] M. P. Desai, G. Caffarena, R. Jevtic, D. G. Márquez, and A. Otero, "A low-latency, low-power FPGA implementation of ECG signal characterization using hermite polynomials," *Electronics*, vol. 10, no. 19, 2021. [Online]. Available: https://www.mdpi.com/2079-9292/10/19/2324

[12] B. U. Demirel, I. A. Bayoumy, and M. A. Al Faruque, "Energy-efficient real-time heart monitoring on edge-fog-cloud internet-of-medical-things," *IEEE Internet of Things Journal*, 2021.

[13] S. Mian Qaisar and A. Subasi, "Cloud-based ECG monitoring using event-driven ECG acquisition and machine learning techniques," *Physical and Engineering Sciences in Medicine*, vol. 43, no. 2, pp. 623–634, 2020.

[14] D. Sanders, L. Ungar, M. A. Eskander, and A. H. Seto, "Ambulatory ECG monitoring in the age of smartphones," *Clevel. Clin. J. Med*, vol. 86, pp. 483–493, 2019.

[15] H. Banaee, M. U. Ahmed, and A. Loutfi, "Data mining for wearable sensors in health monitoring systems: A review of recent trends and challenges," *Sensors*, vol. 13, no. 12, pp. 17 472–17 500, 2013.

[16] H. Kim, S. Kim, N. Van Helleputte, A. Artes, M. Konijnenburg, J. Huisken, C. Van Hoof, and R. F. Yazicioglu, "A configurable and low-power mixed signal SoC for portable ECG monitoring applications," *IEEE Transactions on Biomedical Circuits and Systems*, vol. 8, no. 2, pp. 257–267, 2013.

[17] A. Martín-Yebra, F. Landreani, C. Casellato, E. Pavan, C. Frigo, P.-F. Migeotte, and E. G. Caiani, "Studying heart rate variability from ballistocardiography acquired by force platform: Comparison with conventional ECG," in *2015 Computing in Cardiology Conference (CinC)*. IEEE, 2015, pp. 929–932.

[18] J. Tejedor, C. A. García, D. G. Márquez, R. Raya, and A. Otero, "Multiple physiological signals fusion techniques for improving heartbeat

detection: A review," *Sensors*, vol. 19, no. 21, 2019. [Online]. Available: https://www.mdpi.com/1424-8220/19/21/4708

[19] I. You, K.-K. R. Choo, C.-L. Ho *et al.*, "A smartphone-based wearable sensors for monitoring real-time physiological data," *Computers & Electrical Engineering*, vol. 65, pp. 376–392, 2018.

[20] A. Mishra, A. Kumari, P. Sajit, and P. Pandey, "Remote web based ECG Monitoring using MQTT Protocol for IoT in healthcare," *Development*, vol. 5, no. 04, 2018.

[21] L. Wang, Y. Hsiao, X. Xie, and S. Lee, "An outdoor intelligent healthcare monitoring device for the elderly," *IEEE Transactions on Consumer Electronics*, vol. 62, no. 2, pp. 128–135, May 2016.

[22] C. L. Herry, M. Frasch, A. J. Seely, and H.-t. Wu, "Heart beat classification from single-lead ECG using the synchrosqueezing transform," *Physiological Measurement*, vol. 38, no. 2, p. 171, 2017.

[23] S. M. Mathews, C. Kambhamettu, and K. E. Barner, "A novel application of deep learning for single-lead ECG classification," *Computers in Biology and Medicine*, vol. 99, pp. 53–62, 2018.

[24] A. Walinjkar and J. Woods, "ECG classification and prognostic approach towards personalized healthcare," in *2017 International Conference on Social Media, Wearable and Web Analytics (Social Media)*. IEEE, 2017, pp. 1–8.

[25] F. Pineda-López, A. Martínez-Fernández, J. L. Rojo-Álvarez, A. García-Alberola, and M. Blanco-Velasco, "A flexible 12-lead/holter device with compression capabilities for low-bandwidth mobile-ECG telemedicine applications," *Sensors*, vol. 18, no. 11, p. 3773, 2018.

[26] A. Němcová, R. Smíšek, L. Maršánová, L. Smital, and M. Vítek, "A comparative analysis of methods for evaluation of ECG signal quality after compression," *BioMed Research International*, 2018.

[27] U. Satija, B. Ramkumar, and M. S. Manikandan, *A review of signal processing techniques for electrocardiogram signal quality assessment*, 2018, vol. 11, pp. 36–52.

[28] A. Page, O. Kocabas, T. Soyata, M. Aktas, and J.-P. Couderc, "Cloud-based privacy-preserving remote ECG monitoring and surveillance," *Annals of Noninvasive Electrocardiology*, vol. 20, no. 4, pp. 328–337, 2015. [Online]. Available: https://onlinelibrary.wiley.com/doi/abs/10.1111/anec.12204

[29] P. T. Dao, X. J. Li, and H. N. Do, "Lossy compression techniques for EEG signals," in *2015 International Conference on Advanced Technologies for Communications (ATC)*. IEEE, 2015, pp. 154–159.

[30] P. Kavitha, "A survey on lossless and lossy data compression methods," *International Journal of Computer Science & Engineering Technology*, vol. 7, no. 03, pp. 110–114, 2016.

[31] Y.-C. Wang, "Data compression techniques in wireless sensor networks," *Pervasive Computing*, vol. 61, no. 1, pp. 75–77, 2012.

[32] A. N. Kahdim and M. E. Manaa, “Design an efficient Internet of Things data compression for healthcare applications,” *Bulletin of Electrical Engineering and Informatics*, vol. 11, no. 3, pp. 1678–1686, 2022.

[33] A. Anand, A. K. Singh, Z. Lv, and G. Bhatnagar, “Compression-then-encryption-based secure watermarking technique for smart healthcare system,” *IEEE MultiMedia*, vol. 27, no. 4, pp. 133–143, 2020.

[34] A. Siddique, O. Hasan, F. Khalid, and M. Shafique, “Approxcs: Near-sensor approximate compressed sensing for IoT-healthcare systems,” *arXiv preprint arXiv:1811.07330*, 2018.

[35] C. Jha and M. Kolekar, “Electrocardiogram data compression techniques for cardiac healthcare systems: A methodological review,” *IRBM*, vol. 43, no. 3, pp. 217–228, 2022. [Online]. Available: https://www.sciencedirect.com/science/article/pii/S1959031821000750

[36] P. Goel and D. L. James, “Unified many-worlds browsing of arbitrary physics-based animations,” *ACM Transactions on Graphics (TOG)*, vol. 41, no. 4, pp. 1–15, 2022.

[37] S. Khan, S. Nazir, A. Hussain, A. Ali, and A. Ullah, “An efficient jpeg image compression based on haar wavelet transform, discrete cosine transform, and run length encoding techniques for advanced manufacturing processes,” *Measurement and Control*, vol. 52, no. 9-10, pp. 1532–1544, 2019.

[38] P. Kanani and M. Padole, “Improving pattern matching performance in genome

sequences using run length encoding in distributed Raspberry Pi clustering environment," *Procedia Computer Science*, vol. 171, pp. 1670–1679, 2020.

[39] B. Bent, B. Lu, J. Kim, and J. P. Dunn, "Biosignal compression toolbox for digital biomarker discovery," *Sensors*, vol. 21, no. 2, p. 516, 2021.

[40] J. Wilson, N. Najjar, J. Hare, and S. Gupta, "Human activity recognition using LZW-coded probabilistic finite state automata," in *2015 IEEE International Conference on Robotics and Automation (ICRA)*, 2015, pp. 3018–3023.

[41] A. Limaye and T. Adegbija, "Hermit: A benchmark suite for the Internet of Medical Things," *IEEE Internet of Things Journal*, vol. 5, no. 5, pp. 4212–4222, 2018.

[42] R. Patel and E. G. Friedman, "Arithmetic encoding for memristive multi-bit storage," in *2012 IEEE/IFIP 20th International Conference on VLSI and System-on-Chip (VLSI-SoC)*. IEEE, 2012, pp. 99–104.

[43] U. Sharma, M. Sood, E. Puthooran, and Y. Kumar, "A block-based arithmetic entropy encoding scheme for medical images," *International Journal of Healthcare Information Systems and Informatics (IJHISI)*, vol. 15, no. 3, pp. 65–81, 2020.

[44] P. Aparna and P. V. V. Kishore, "Biometric-based efficient medical image watermarking in e-healthcare application," *IET Image Processing*, vol. 13, no. 3, pp. 421–428, 2019.

[45] F. M. Kaffah, Y. A. Gerhana, I. M. Huda, A. Rahman, K. Manaf, and B. Subaeki, “E-mail message encryption using Advanced Encryption Standard (AES) and Huffman compression engineering,” pp. 1–6, 2020.

[46] Z. Cao, Y. Li, J. Peng, G. Chai, and G. Zhao, “Controlled quantum secure direct communication protocol based on huffman compression coding,” *International Journal of Theoretical Physics*, vol. 57, no. 12, pp. 3632–3642, 2018.

[47] A. Gopinath and M. Ravisankar, “Comparison of lossless data compression techniques,” in *2020 International Conference on Inventive Computation Technologies (ICICT)*, 2020, pp. 628–633.

[48] P. Kuppusamy, R. Sureshkumar, S. Yuvaraj, and E. Dilliraj, “VLSI based lossless ECG compression algorithm implementation for low power devices,” in *Journal of Physics: Conference Series*, vol. 1964, no. 6, 2021, p. 062073.

[49] C.-I. Ieong, M. Li, M.-K. Law, P.-I. Mak, M. I. Vai, and R. P. Martins, “A 0.45 v 147–375 NW ECG compression processor with wavelet shrinkage and adaptive temporal decimation architectures,” *IEEE Transactions on Very Large Scale Integration (VLSI) Systems*, vol. 25, no. 4, pp. 1307–1319, 2017.

[50] G. C. Chang and Y. D. Lin, “An efficient lossless ECG compression method using Delta coding and optimal selective Huffman coding,” in *6th World Congress of Biomechanics (WCB 2010), Singapore.* Springer Berlin Heidelberg, 2010.

[51] G. Pekhimenko, V. Seshadri, O. Mutlu, M. A. Kozuch, P. B. Gibbons, and T. C.

Mowry, "Base-delta-immediate compression: Practical data compression for on-chip caches," in *2012 21st International Conference on Parallel Architectures and Compilation Techniques (PACT)*, 2012, pp. 377–388.

[52] A. Mincholé, J. Camps, A. Lyon, and B. Rodríguez, "Machine learning in the Electrocardiogram," *Journal of Electrocardiology*, vol. 57, pp. S61–S64, 2019.

[53] M. Wasimuddin, K. Elleithy, A.-S. Abuzneid, M. Faezipour, and O. Abuzaghleh, "Stages-based ECG signal analysis from traditional signal processing to machine learning approaches: A survey," *IEEE Access*, vol. 8, pp. 177 782–177 803, 2020.

[54] E. J. d. S. Luz, W. R. Schwartz, G. Cámara-Chávez, and D. Menotti, "ECG-based heartbeat classification for arrhythmia detection: A survey," *Computer Methods and Programs in Biomedicine*, vol. 127, pp. 144–164, 2016.

[55] A. Kumar and M. Singh, "Ischemia detection using isoelectric energy function," *Computers in Biology and Medicine*, vol. 68, pp. 76–83, 2016.

[56] R. Firoozabadi, R. E. Gregg, and S. Babaeizadeh, "Modeling and classification of the ST segment morphology for enhanced detection of acute myocardial infarction," in *2019 Computing in Cardiology (CinC)*. IEEE, 2019, pp. Page–1.

[57] T. Li and M. Zhou, "ECG classification using wavelet packet entropy and random forests," *Entropy*, vol. 18, no. 8, p. 285, 2016.

[58] S. Ansari, N. Farzaneh, M. Duda, K. Horan, H. B. Andersson, Z. D. Goldberger, B. K. Nallamothu, and K. Najarian, "A review of automated methods for detection of myocardial ischemia and infarction using electrocardiogram and

electronic health records," *IEEE Reviews in Biomedical Engineering*, vol. 10, pp. 264–298, 2017.

[59] C. Venkatesan, P. Karthigaikumar, A. Paul, S. Satheeskumaran, and R. Kumar, "ECG signal preprocessing and SVM classifier-based abnormality detection in remote healthcare applications," *IEEE Access*, vol. 6, pp. 9767–9773, 2018.

[60] C. K. Jha and M. H. Kolekar, "Cardiac arrhythmia classification using tunable q-wavelet transform based features and support vector machine classifier," *Biomedical Signal Processing and Control*, vol. 59, p. 101875, 2020.

[61] C. T. Arsene, R. Hankins, and H. Yin, "Deep learning models for denoising ECG signals," in *2019 27th European Signal Processing Conference (EUSIPCO)*. IEEE, 2019, pp. 1–5.

[62] X. Liu, H. Wang, Z. Li, and L. Qin, "Deep learning in ECG diagnosis: A review," *Knowledge-Based Systems*, 2021. [Online]. Available: https://www.sciencedirect.com/science/article/pii/S0950705121004494

[63] G. Sannino and G. De Pietro, "A deep learning approach for ECG-based heartbeat classification for arrhythmia detection," *Future Generation Computer Systems*, vol. 86, pp. 446–455, 2018.

[64] Z. Ebrahimi, M. Loni, M. Daneshtalab, and A. Gharehbaghi, "A review on deep learning methods for ECG arrhythmia classification," *Expert Systems with Applications: X*, vol. 7, p. 100033, 2020.

[65] J. Wu, F. Li, Z. Chen, Y. Pu, and M. Zhan, "A neural network-based ECG

classification processor with exploitation of heartbeat similarity," *IEEE Access*, vol. 7, pp. 172 774–172 782, 2019.

[66] M. Janveja, R. Parmar, M. Tantuway, and G. Trivedi, "A DNN-based low power ECG co-processor architecture to classify cardiac arrhythmia for wearable devices," *IEEE Transactions on Circuits and Systems II: Express Briefs*, vol. 69, no. 4, pp. 2281–2285, 2022.

[67] F. Corradi, S. Pande, J. Stuijt, N. Qiao, S. Schaafsma, G. Indiveri, and F. Catthoor, "ECG-based heartbeat classification in neuromorphic hardware," in *2019 International Joint Conference on Neural Networks (IJCNN)*, 2019, pp. 1–8.

[68] I. Monedero, "A novel ECG diagnostic system for the detection of 13 different diseases," *Engineering Applications of Artificial Intelligence*, vol. 107, p. 104536, 2022.

[69] G. Sivapalan, K. K. Nundy, S. Dev, B. Cardiff, and D. John, "Annet: A lightweight neural network for ECG anomaly detection in IoT edge sensors," *IEEE Transactions on Biomedical Circuits and Systems*, vol. 16, no. 1, pp. 24–35, 2022.

[70] K. Guk, G. Han, J. Lim, K. Jeong, T. Kang, E.-K. Lim, and J. Jung, "Evolution of wearable devices with real-time disease monitoring for personalized healthcare," *Nanomaterials*, vol. 9, no. 6, p. 813, 2019.

[71] G. Cosoli, S. Spinsante, F. Scardulla, L. D'Acquisto, and L. Scalise, "Wireless ECG and cardiac monitoring systems: State of the art, available commercial

devices and useful electronic components," *Measurement*, vol. 177, p. 109243, 2021. [Online]. Available: https://www.sciencedirect.com/science/article/pii/S0263224121002542

[72] H. Yu, N. Li, and N. Zhao, "How far are we from achieving self-powered flexible health monitoring systems: An energy perspective," *Advanced Energy Materials*, vol. 11, no. 9, p. 2002646, 2021.

[73] S. Ramasamy and A. Balan, "Wearable sensors for ECG measurement: A review," *Sensor Review*, 2018.

[74] Khan, Yasser and Thielens, Arno and Muin, Sifat and Ting, Jonathan and Baumbauer, Carol and Arias, Ana C., "A new frontier of printed electronics : flexible hybrid electronics," *Advanced Materials*, vol. 32, no. 15, p. 29, 2020. [Online]. Available: {http://dx.doi.org/10.1002/adma.201905279}

[75] K. Tripathi, H. Sohal, and S. Jain, "Design and implementation of robust low power ECG pre-processing module," *IETE Journal of Research*, pp. 1–7, 2020.

[76] S. M. Noor, E. John, and M. Panday, "Design and implementation of an ultralow-energy FFT ASIC for processing ECG in cardiac pacemakers," *IEEE Transactions on Very Large Scale Integration (VLSI) systems*, vol. 27, no. 4, pp. 983–987, 2018.

[77] T. J. Jun, H. M. Nguyen, D. Kang, D. Kim, D. Kim, and Y.-H. Kim, "ECG arrhythmia classification using a 2-D convolutional neural network," *arXiv preprint arXiv:1804.06812*, 2018.

[78] J. Li, M. Bhuiyan, X. Huang, B. McDonald, T. Farrell, and E. Clancy, "Reducing electric power consumption when transmitting ECG/EMG/EEG using a bluetooth low energy microcontroller," in *2018 IEEE Signal Processing in Medicine and Biology Symposium (SPMB)*. IEEE, 2018, pp. 1–3.

[79] K. Badami, M. Pons-Sole, E. Azarkhish, A. Fivaz, M. Rapin, O. Chételat, and S. Emery, "Single-battery cooperative sensors for multi-lead long term ambulatory ECG measurement," in *2021 IEEE Biomedical Circuits and Systems Conference (BioCAS)*. IEEE, 2021, pp. 1–4.

[80] Q. Yang, A. Chen, C. Li, G. Zou, H. Li, and C. Zhi, "Categorizing wearable batteries: Unidirectional and omnidirectional deformable batteries," *Matter*, vol. 4, no. 10, pp. 3146–3160, 2021.

[81] I. Mathews, S. N. Kantareddy, T. Buonassisi, and I. M. Peters, "Technology and market perspective for indoor photovoltaic cells," *Joule*, vol. 3, no. 6, pp. 1415–1426, 2019.

[82] Y. Cui, B. Wang, and K. Wang, "Energy conversion performance optimization and strength evaluation of a wearable thermoelectric generator made of a thermoelectric layer on a flexible substrate," *Energy*, vol. 229, p. 120694, 2021.

[83] A. Tiwari and T. H. Falk, "Lossless electrocardiogram signal compression: A review of existing methods," *Biomedical Signal Processing and Control*, vol. 51, pp. 338–346, 2019.

[84] A. Moon, S. Woo Son, J. Jung, and Y. Jeong Song, "Understanding bit-error trade-off of transform-based lossy compression on electrocardiogram signals,"

in *2020 IEEE International Conference on Big Data (Big Data)*, 2020, pp. 3494–3499.

[85] L. Rebollo-Neira, “Effective high compression of ecg signals at low level distortion,” *Scientific reports*, vol. 9, no. 1, pp. 1–12, 2019.

[86] T.-H. Tsai and W.-T. Kuo, “An efficient ecg lossless compression system for embedded platforms with telemedicine applications,” *IEEE Access*, vol. 6, pp. 42 207–42 215, 2018.

[87] C. J. Deepu, C.-H. Heng, and Y. Lian, “A hybrid data compression scheme for power reduction in wireless sensors for IoT,” *IEEE transactions on biomedical circuits and systems*, vol. 11, no. 2, pp. 245–254, 2016.

[88] B.-H. Kung, P.-Y. Hu, C.-C. Huang, C.-C. Lee, C.-Y. Yao, and C.-H. Kuan, “An efficient ECG classification system using resource-saving architecture and random forest,” *IEEE Journal of Biomedical and Health Informatics*, vol. 25, no. 6, pp. 1904–1914, 2020.

[89] X. Li, R. Panicker, B. Cardiff, and D. John, “Multistage pruning of CNN based ECG classifiers for edge devices,” *arXiv preprint arXiv:2109.00516*, 2021.

[90] N. Wang, J. Zhou, G. Dai, J. Huang, and Y. Xie, “Energy-efficient intelligent ECG monitoring for wearable devices,” *IEEE Transactions on Biomedical Circuits and Systems*, vol. 13, no. 5, pp. 1112–1121, 2019.

[91] M. A. Scrugli, D. Loi, L. Raffo, and P. Meloni, “An adaptive cognitive sensor node for ECG monitoring in the Internet of Medical Things,” *IEEE Access*, vol. 10, pp. 1688–1705, 2021.

[92] N. T. Bui, T. H. Vo, B.-G. Kim, and J. Oh, “Design of a solar-powered portable ECG device with optimal power consumption and high accuracy measurement,” *Applied Sciences*, vol. 9, no. 10, p. 2129, 2019.

[93] V. S. Naresh, S. S. Pericherla, P. S. R. Murty, and R. Sivaranjani, “Internet of Things in healthcare: Architecture, applications, challenges, and solutions.” *Computer Systems Science and Engineering* , vol. 35, no. 6, pp. 411–421, 2020.

[94] H. Ouda, A. Badr, A. Rashwan, H. S. Hassanein, and K. Elgazzar, “Optimizing real-time ecg data transmission in constrained environments,” in *ICC 2022-IEEE International Conference on Communications.* IEEE, 2022, pp. 2114–2119.

[95] “HE Instruments TechPatient CARDIO V4 ECG Simulator,” https://www.heinstruments.com.

[96] T. H. Institute, “Categories of arrhythmias,” https://www.texasheart.org/heart-health/heart-information-center/topics/categories-of-arrhythmias/.

[97] M. Clinic-Arrhythmia, “Heart arrhythmia,” https://www.mayoclinic.org/diseases-conditions/heart-arrhythmia/symptoms-causes/syc-20350668.

[98] M. Clinic-Ischemia, “Myocardial ischemia,” https://www.mayoclinic.org/diseases-conditions/myocardial-ischemia/symptoms-causes/syc-20375417.

[99] A. M. Training, “ECGs in acute myocardial infarction,” https://www.aclsmedicaltraining.com/ecg-in-acute-myocardial-infarction/.

[100] J. H. Medicine, “Heart block,” https://www.hopkinsmedicine.org/health/conditions-and-diseases/heart-block.

[101] C. Clinic, "Heart block," https://my.clevelandclinic.org/health/diseases/17056-heart-block.

[102] J. F. Saenz-Cogollo and M. Agelli, "Investigating feature selection and random forests for inter-patient heartbeat classification," *Algorithms*, vol. 13, no. 4, 2020. [Online]. Available: https://www.mdpi.com/1999-4893/13/4/75

[103] A. Badr, A. Badawi, A. Rashwan, and K. Elgazzar, "12-lead ecg platform for real-time monitoring and early anomaly detection," in *2022 International Wireless Communications and Mobile Computing (IWCMC)*. IEEE, 2022, pp. 973–978.

[104] G. Moody and R. Mark, "The impact of the MIT-BIH arrhythmia database," *IEEE Engineering in Medicine and Biology Magazine*, vol. 20, no. 3, pp. 45–50, 2001.

[105] G. Doquire, G. De Lannoy, D. François, and M. Verleysen, "Feature selection for interpatient supervised heart beat classification," *Computational Intelligence and Neuroscience*, 2011.

[106] I. C. S. M. W. MCU". Accessed on: January, 2022. [online]. available: https://www.ti.com/lit/ds/symlink/cc2650.pdf.

[107] H. Ouda, A. Badawi, K. Elgazzar, and H. Hassanein, "Energy saving on constrained 12-leads real-time ecg monitoring," *GLOBECOM Conference 2022 (Accepted)*.

[108] A. Y. Hannun, P. Rajpurkar, M. Haghpanahi, G. H. Tison, C. Bourn, M. P.

Turakhia, and A. Y. Ng, “Cardiologist-level arrhythmia detection and classification in ambulatory electrocardiograms using a deep neural network,” *Nature Medicine*, vol. 25, no. 1, pp. 65–69, 2019.

[109] Stanford ML - Deep Neural Networks for ECG Rhythm Classification, https://irhythm.github.io/cardiol_test_set/.

[110] M. P. Turakhia, D. D. Hoang, P. Zimetbaum, J. D. Miller, V. F. Froelicher, U. N. Kumar, X. Xu, F. Yang, and P. A. Heidenreich, “Diagnostic utility of a novel leadless arrhythmia monitoring device,” *The American Journal of Cardiology*, vol. 112, no. 4, pp. 520–524, 2013.

[111] E. Waves-RBBB, “Right bundle branch block,” https://ecgwaves.com/topic/right-bundle-branch-block-rbbb-ecg-criteria-treatment/.

[112] E. Waves-LBBB, “Left bundle branch block,” https://ecgwaves.com/topic/left-bundle-branch-block-lbbb-ecg-criteria-treatment/.

[113] A. H. Ribeiro, M. H. Ribeiro, G. M. Paixão, D. M. Oliveira, P. R. Gomes, J. A. Canazart, M. P. Ferreira, C. R. Andersson, P. W. Macfarlane, W. Meira Jr *et al.*, “Automatic diagnosis of the 12-lead ECG using a deep neural network,” *Nature communications*, vol. 11, no. 1, pp. 1–9, 2020.

[114] C. test: An annotated 12-lead ECG dataset, https://doi.org/10.5281/zenodo.3765780.

[115] J. F. A. A. C. System and Disorders, “Sinus bradycardia,” https://johnsonfrancis.org/professional/sinus-bradycardia-on-ecg/.

[116] E. Waves-ST, "Sinus tachycardia," https://ecgwaves.com/topic/sinus-tachycardia-causes-ecg-inappropriate-management/.